J. Plasma Phys. (2017), *vol.* 83, 705830102
doi:10.1017/S0022377816001197

Diagnosing collisionless energy transfer using field–particle correlations: Vlasov–Poisson plasmas

Gregory G. Howes[1,†], **Kristopher G. Klein**[2,3] **and Tak Chu Li**[1]

[1]Department of Physics and Astronomy, University of Iowa, Iowa City, IA 52242, USA

[2]Department of Climate and Space Sciences and Engineering, University of Michigan, Ann Arbor, MI 48109, USA

[3]Space Science Center, University of New Hampshire, Durham, NH 03824, USA

(Received 24 June 2016; revised 29 November 2016; accepted 1 December 2016)

Turbulence plays a key role in the conversion of the energy of large-scale fields and flows to plasma heat, impacting the macroscopic evolution of the heliosphere and other astrophysical plasma systems. Although we have long been able to make direct spacecraft measurements of all aspects of the electromagnetic field and plasma fluctuations in near-Earth space, our understanding of the physical mechanisms responsible for the damping of the turbulent fluctuations in heliospheric plasmas remains incomplete. Here we propose an innovative field–particle correlation technique that can be used to measure directly the secular energy transfer from fields to particles associated with collisionless damping of the turbulent fluctuations. Furthermore, this novel procedure yields information about the collisionless energy transfer as a function of particle velocity, providing vital new information that can help to identify the dominant collisionless mechanism governing the damping of the turbulent fluctuations. Kinetic plasma theory is used to devise the appropriate correlation to diagnose Landau damping, and the field–particle correlation technique is thoroughly illustrated using the simplified case of the Landau damping of Langmuir waves in a 1D-1V (one dimension in physical space and one dimension in velocity space) Vlasov–Poisson plasma. Generalizations necessary to apply the field–particle correlation technique to diagnose the collisionless damping of turbulent fluctuations in the solar wind are discussed, highlighting several caveats. This novel field–particle correlation technique is intended to be used as a primary analysis tool for measurements from current, upcoming and proposed spacecraft missions that are focused on the kinetic microphysics of weakly collisional heliospheric plasmas, including the Magnetospheric Multiscale (MMS), Solar Probe Plus, Solar Orbiter and Turbulence Heating ObserveR (THOR) missions.

Key words: astrophysical plasmas, plasma nonlinear phenomena, space plasma physics

1. Introduction

The flow of energy from the sun, through interplanetary space, to the magnetospheres of the Earth and other planets impacts the macroscopic evolution of the heliosphere,

† Email address for correspondence: gregory-howes@uiowa.edu

our home in the universe. Plasma turbulence plays a key role in this process, mediating the conversion of the energy of large-scale fields and flows to plasma heat. But our understanding of how turbulence governs energy transport and plasma heating remains incomplete, representing a grand challenge problem in heliophysics.

To complicate matters further, in many turbulent heliospheric plasmas of interest, such as the solar corona and the solar wind, the typically low-density and high-temperature conditions dictate that the turbulent dynamics is weakly collisional, requiring the application of kinetic plasma theory to follow the evolution and dissipation of the turbulence. Kinetic plasma theory describes the evolution of six-dimensional (6-D, or 3D-3V) particle velocity distribution functions and the resulting electromagnetic fields, so in addition to tackling the large spatial dynamic range typical of turbulence problems, heliospheric plasma turbulence demands novel theoretical approaches to tackle the inherently high dimensionality of the kinetic plasma dynamics. A particular challenge at the frontier of studies in kinetic plasma turbulence is to identify the physical mechanisms by which the turbulent electromagnetic field and plasma flow fluctuations are damped and their energy converted to plasma heat, or some other energization of particles.

Under the very low collisionality typical of the solar corona and solar wind, the damping of the turbulent fluctuations is governed by collisionless interactions between the electromagnetic fields and the plasma particles. In linear kinetic theory, such interactions lead to the collisionless damping of linear waves and are therefore commonly denoted wave–particle interactions, with typical examples being Landau damping (Landau 1946; Villani 2014), transit-time damping (Barnes 1966) and cyclotron damping (Stix 1992). It is important to note that the underlying physical process occurring in such wave–particle interactions is not limited to linearized systems or to sinusoidal waveforms, but holds as well for nonlinearly evolving plasmas. For a turbulent plasma, in which nonlinear evolution plays a central role, the collisionless interactions between the electromagnetic fields and the plasma particles may lead to a secular transfer of energy from fields to particles, resulting in collisionless damping of the turbulent fluctuations. Recognizing that the linearization and plane-wave decomposition frequently adopted in analytical calculations are often simply chosen to express the essential collisionless dynamics in a simplified context, we choose to adopt here the term wave–particle interaction as a general concept not limited to a linearized system.

Although handling the three additional dimensions of velocity space inherent to kinetic theory is a significant challenge, both analytically and numerically, the fluctuations in velocity space constitute a new source of information about the dynamics and energetics of a turbulent kinetic plasma. Although the interpretation of velocity-space data is not straightforward in many cases, it represents a largely untapped potential source of information for discovery science. Although direct sampling of turbulence in the solar wind by spacecraft missions is often limited to measurements at a single point in space as a function of time, spacecraft can also provide measurements of the three-dimensional particle velocity distribution (3V) at that position in space as a function of time.

Our ultimate goal is to devise a strategy to identify and characterize the secular transfer of energy from fields to particles (leading to the collisionless damping of the turbulent fluctuations) using measurements of the electromagnetic fields and particle velocity distributions at a single point in space as a function of time. In particular, how this energy transfer varies as a function of particle velocity illuminates the properties of the collisionless energy transfer, potentially helping to identify definitively the

https://doi.org/10.1017/S0022377816001197 Published online by Cambridge University Press

physical processes involved in the damping of the turbulence. Here we propose the general concept of using field–particle correlations to isolate the net transfer of energy from fields to particles as turbulent fluctuations are damped through collisionless interactions between the electromagnetic fields and individual plasma particles.

In this paper, we employ the simplified 1D-1V (one dimension in physical space and one dimension in velocity space) Vlasov–Poisson system for the nonlinear evolution of electrostatic fluctuations in an unmagnetized plasma to guide the development of a procedure to identify the secular energy transfer via collisionless wave–particle interactions. We propose an innovative analysis technique using field–particle correlations at a single point in space to estimate the energization of the plasma particles due to the damping of the electromagnetic fields, providing vital new information about how this energy transfer is distributed as a function of particle velocity. We employ nonlinear simulations of the 1D-1V system to illustrate the application of this novel procedure.

As the intended application of this technique is to diagnose the collisionless energy transfer between turbulent electromagnetic fluctuations and particles in weakly collisional heliospheric and astrophysical environments, such as the solar wind and solar corona, we choose parameters for this simple numerical demonstration of the technique most relevant to the case of solar wind turbulence. Since the turbulent fluctuations in the solar wind typically have $|\delta \boldsymbol{B}|/|\boldsymbol{B}| \sim 0.1$ at the kinetic length scales on which the turbulent fluctuations may be collisionlessly damped, we choose the amplitudes of the damped Langmuir waves to be $\delta n/n_0 \sim 0.1$. At these amplitudes, quasilinear theory describes quite accurately the evolution of the system, which primarily shows damping of the initial Langmuir waves. The emergence of strongly nonlinear features in phase space, such as BGK (Bernstein–Greene–Kruskal) structures or phase-space vortices, requires significantly higher initial amplitudes of $\delta n/n_0 \gtrsim 0.5$. Although the application of the field–particle correlation technique to analyse the collisionless energy transfer in such a strongly nonlinear regime would potentially be very interesting, it is not directly relevant to the parameter regime of solar wind turbulence, so we do not explore this limit of strong nonlinearity in the 1D-1V Vlasov–Poisson system. Subsequent work will generalize the application of the field–particle correlation technique to the case of turbulent electromagnetic fluctuations in a magnetized plasma directly relevant to many heliospheric and astrophysical environments.

1.1. *Previous investigations of waves and particles*

The idea of examining the relation between measured electromagnetic fields and particle fluxes in weakly collisional space plasmas has long been used in the investigation of the energy transfer between fields and particles. The types of studies that have been performed in the past fall into three broad categories: (i) spatial coincidence, (ii) conjunction and (iii) correlation. In spatial coincidence studies, if a single spacecraft measures a feature in both the fields and particles at the same time – for example, a particular feature in the frequency spectrum along with an enhancement of particle counts within a certain energy and pitch angle bin – this evidence is used to infer the action of wave–particle interactions. In conjunction studies (Keiling 2009), the measurements at different positions along the same magnetic flux tube can be used to infer the integrated effect of wave–particle interactions between the two points. In correlation studies, a mathematical correlation between field measurements and particle measurements is performed using measurements at the same point in

https://doi.org/10.1017/S0022377816001197 Published online by Cambridge University Press

space, preserving the valuable phase information needed to establish definitively an interaction between the fields and particles.

Spatial coincidence studies between measured field fluctuations and particle fluxes have played an important role since the early exploration of the physical phenomena in the Earth's magnetosphere. Bursts of energetic electrons with $E \geqslant 40$ keV measured by the Injun 3 spacecraft were found to be accompanied by the very low frequency (VLF) electromagnetic fluctuations of the whistler-mode chorus (Oliven & Gurnett 1968), and subsequent studies using high-altitude balloons (Rosenberg, Helliwell & Katsufrakis 1971) and the Ogo 5 satellite (Burton & Holzer 1974) found further evidence of association between the distribution of energetic electrons in the range from 40 keV $\leqslant E \leqslant$ 100 keV and whistler chorus emissions (Kennel & Petschek 1966). In addition, spatial coincidence studies also provided evidence linking electrostatic fluctuations above the cyclotron frequency to diffusion and pitch angle scattering of energetic electrons in the region $5 \lesssim L \lesssim 7$ (Kennel *et al.* 1970; Fredricks & Scarf 1973; Scarf *et al.* 1973; Shaw & Gurnett 1975). Subsequent work using measurements from the Explorer 45 spacecraft showed that electrons with energies 1 keV $\leqslant E \leqslant$ 10 keV injected during magnetic storms and substorms appeared to be associated with VLF emissions both above and below the cyclotron frequency (Anderson & Maeda 1977).

Early magnetic conjunction studies included the comparison of ground-based measurements of VLF radio waves at high latitudes (Siple, Antarctica, which samples magnetic field lines $L \simeq 4$) to *in situ* electron measurements on the geostationary ATS 6 satellite (Park, Parks & Lin 1981) and the launching of VLF waves from the same ground station with observations made by the Japanese EXOS-B satellite (Kimura *et al.* 1983).

Magnetic conjunction studies are particularly well suited to study the interaction of particles with electromagnetic waves that travel primarily along the magnetic field, such as the Alfvén wave and its kinetic counterparts. Travelling along the Earth's magnetic field from the distant magnetosphere toward the ionosphere below, Alfvén waves play a key role in the coupling of the magnetosphere–ionosphere system (Keiling 2009). Alfvén waves can be launched by a sheared plasma flow perpendicular to Earth's magnetic field, or by a sudden dynamic change in convection or resistivity in some region of the magnetosphere (Stasiewicz *et al.* 2000), as can occur when magnetic storms cause shifts in magnetospheric boundaries or when magnetotail reconnection occurs (Hasegawa 1976). When these Earth-bound waves pass a geocentric radius of $r \sim 3R_E$, the cold plasma of primarily ionospheric origin and strong magnetic field of the Earth lead to plasma conditions in the inertial regime, with $\beta < m_e/m_i$ or $v_{te} < v_A$, and Alfvén waves with small cross-field scales transition to inertial Alfvén waves (Lysak & Lotko 1996; Stasiewicz *et al.* 2000). Associated with the inertial Alfvén wave is a significant component of the electric field parallel to the local magnetic field, and this parallel electric field has been proposed as a primary mechanism for the acceleration of auroral electrons (Hasegawa 1976; Goertz & Boswell 1979; Lysak & Dum 1983; Hui & Seyler 1992; Kletzing 1994; Lysak & Lotko 1996).

Subsequently, the FAST, Freja, Polar, DMSP, Geotail and Cluster missions have provided unparalleled new opportunities to use magnetic conjunction studies to explore the Alfvénic electron acceleration in the auroral zone. Polar measurements of downward Alfvénic Poynting flux at 4–7 R_E in the plasma sheet boundary layer (PSBL) are closely associated with the luminosity of magnetically conjugate auroral structures in a statistical study of 40 PSBL crossings (Keiling *et al.* 2002). A study

https://doi.org/10.1017/S0022377816001197 Published online by Cambridge University Press

of the conjunctions of the Polar spacecraft at 4–7 R_E and the FAST spacecraft at 1.05–1.65 R_E demonstrated statistically that the Alfvénic Poynting flux dominated over electron energy flux at Polar orbits but the electron energy flux was greater than the Alfvénic Poynting flux at the FAST altitudes (Chaston *et al.* 2003; Chaston 2006). This evidence supports the picture that Alfvén waves are losing energy via wave–particle interactions to accelerate electrons as they propagate toward the ionosphere. A statistical survey correlating particle fluxes and Alfvén wave fields of more than 5000 polar orbits from the FAST satellite shows that Alfvén waves may be responsible for 31 % of all auroral activity (Chaston *et al.* 2007). At magnetic local noon and midnight, Alfvénic activity may account for as much as 50 % of auroral activity. Finally, Schriver *et al.* (Schriver *et al.* 2003) used seven FAST–Polar conjunction events to show that, during geomagnetically active times, Polar measured large-amplitude Alfvén waves in the PSBL, FAST measured field-aligned electron acceleration events and the Polar Ultraviolet Imager (UVI) recorded strong auroral luminosity at the magnetically conjugate point in the ionosphere. They concluded that Alfvén waves are important drivers of auroral acceleration, in addition to quasi-static, field-aligned potentials and the earthward flow of energetic plasma beams from the magnetotail.

Although the magnetic conjunction studies above have provided significant insights into the dynamics of wave–particle interactions in the auroral magnetosphere, all conjunction studies suffer from difficulties such as field line mapping, differential motions of the field lines at each spacecraft, different orbital speeds of the spacecraft and time delays in signal propagation along the field lines (Keiling 2009). Furthermore, conjunction studies, in common with spatial coincidence studies, lack the phase information needed to confirm directly the energy transfer between fields and particles. Only correlation studies can provide such a direct estimate of the collisionless energy transfer.

An early attempt to identify wave–particle interactions in space plasmas sought to measure the phase bunching of resonant electrons predicted to occur in the presence of sufficiently large-amplitude Langmuir wave fluctuations (Melrose 1986). Particle auto-correlator instruments were developed to detect electron phase bunching at MHz frequencies in the auroral ionosphere, even when electron count rates are $\lesssim 10^5$ Hz (Spiger *et al.* 1974, 1976; Gough 1980; Gough *et al.* 1980). Although the measurements from these early instruments were merely used to seek the coincidence of phase-bunched electrons with features in the electrostatic wave spectrum, they provided a critical foundation for the subsequent development of wave–particle correlators. The application of electron particle auto-correlators to study wave–particle interactions continued with experiments on later sounding rocket flights (Gough & Urban 1983; Gough, Christiansen & Wilhelm 1990) and with the inception of active experiments, where an electron beam launched by one spacecraft is measured by another and the distortion of that received beam provides a sensitive probe of the physics of wave–particle interactions. Such active experiments where conducted during space shuttle flights using tethered satellites (Gough *et al.* 1995, 1997, 1998*a*,*c*; Huang *et al.* 1998; Burke *et al.* 1999; Rubin *et al.* 1999) and with dual payload sounding rocket flights (Gough, Hardy & James 1998*b*; Huang *et al.* 2001). More recently, all four of the Cluster-II spacecraft were equipped with particle auto-correlators for the electrons (Woolliscroft *et al.* 1997), and early results from measurements by this instrument, as well as a thorough review of previous particle auto-correlator experiments, are presented in Gough *et al.* (2003).

The first true wave–particle correlator, flown on a sounding rocket in the auroral zone, performed a direct correlation of the arrival times of electrons with the phase

https://doi.org/10.1017/S0022377816001197 Published online by Cambridge University Press

of the high-frequency wave field (Ergun *et al.* 1991*a*,*b*). This experiment indeed detected electron phase bunching during periods of intense Langmuir waves, driving subsequent theoretical work to develop refined theoretical predictions for finite-size Langmuir wavepackets (Muschietti, Roth & Ergun 1994). Another wave–particle correlator was flown on the NASA Combined Release and Radiation Effects Satellite (CRRES), computing correlations on board between the Low Energy Plasma Analyzer and the electric field/Langmuir probe instrument (Watkins *et al.* 1996), and later a refined wave–particle correlator was implemented as a component of the Fields instrument on the FAST spacecraft (Ergun, McFadden & Carlson 1998; Ergun *et al.* 2001). Subsequent development lead to an improved wave–particle correlator design with higher phase resolution than previous instruments, flown on an auroral sounding rocket, which measured the reactive component of the electron phase bunching in a Langmuir wave (Kletzing *et al.* 2005; Kletzing & Muschietti 2006). Further developments in wave–particle correlator instrumentation continue (Fukuhara *et al.* 2009), with the planned implementation of an on-board Wave–Particle Interaction Analyzer in the upcoming Japanese Exploration of energization and Radiation in Geospace (ERG) spacecraft mission to study the energy transfer process between energetic electrons and whistler-mode chorus emissions in the Earth's inner magnetosphere (Katoh *et al.* 2013).

All of these wave–particle correlator instruments are specially designed to explore the energy transfer to particles from waves that have frequencies at or above the particle detector counting rate, for example studying the interaction of electrons with whistler waves or Langmuir waves in the Earth's magnetosphere. But the Alfvénic turbulent fluctuations in the solar wind and solar corona have a much lower frequency than the whistler and Langmuir wave fluctuations of interest in the magnetosphere. Furthermore, current, upcoming, and proposed spacecraft missions – such as the Magnetospheric Multiscale (MMS) (Burch *et al.* 2016), Solar Probe Plus (Kasper *et al.* 2015; Bale *et al.* 2016), Solar Orbiter (Müller *et al.* 2013) and Turbulence Heating ObserveR (THOR) (Vaivads *et al.* 2016) missions – boast fast, three-dimensional particle velocity measurements at a sampling rate approaching or surpassing the frequency of the fluctuations involved in the collisionless transfer of energy between fields and particles. For example, collisionless damping of turbulent fluctuations by protons peaks at the ion kinetic scales, coincident with the scale of the spectral break between the inertial and dissipation ranges of the turbulent magnetic energy frequency spectrum in the solar wind, occurring at a spacecraft-frame frequency of approximately $f \sim 0.4$ Hz. The MMS mission samples the 3V proton velocity distribution function with a sampling rate of 150 ms, and the THOR mission proposes the same sampling rate with improved sensitivity, both yielding a Nyquist frequency of $f_{Ny} > 3$ Hz, sufficient to resolve the velocity-space dynamics of the strongly damped fluctuations. Similarly, collisionless damping by electrons is believed to be distributed across a range of scales within the dissipation range (Told *et al.* 2015), corresponding to spacecraft-frame frequencies in the range 1 Hz $\lesssim f \lesssim$ 20 Hz. The MMS mission boasts sampling of 3V electron velocity distribution functions at 30 ms, and the THOR mission proposes electron measurements at a 5 ms sampling rate, corresponding to Nyquist frequencies of $f_{Ny} > 16$ Hz and $f_{Ny} = 100$ Hz respectively, sufficient to resolve the electron velocity-space dynamics of the strongly damped fluctuations. These unprecedented capabilities motivate the development of a thorough foundation of kinetic theory to maximize the scientific return from these missions. The key concept underlying the innovative field–particle correlations proposed here is to exploit the variation of the correlations as a function of the particle velocity to gain much deeper insight into the nature of the collisionless energy transfer mechanism.

https://doi.org/10.1017/S0022377816001197 Published online by Cambridge University Press

2. Physics of energy transfer via collisionless wave–particle interactions

To investigate the dynamics and energetics of turbulence in weakly collisional plasmas relevant to heliospheric environments, such as the solar corona and the solar wind, one may use the Boltzmann equation to describe the evolution of the six-dimensional velocity distribution function $f_s(\boldsymbol{r}, \boldsymbol{v}, t)$ for a plasma species s,

$$\frac{\partial f_s}{\partial t} + \boldsymbol{v} \cdot \nabla f_s + \frac{q_s}{m_s}\left[\boldsymbol{E} + \frac{\boldsymbol{v} \times \boldsymbol{B}}{c}\right] \cdot \frac{\partial f_s}{\partial \boldsymbol{v}} = \left(\frac{\partial f_s}{\partial t}\right)_{coll}. \tag{2.1}$$

Combining the Boltzmann equation for each plasma species together with Maxwell's equations forms the closed set of Maxwell–Boltzmann equations that govern the nonlinear evolution of turbulent fluctuations in a magnetized kinetic plasma.

Under the weakly collisional conditions typical of turbulent heliospheric plasmas, the collisional term on the right-hand side of (2.1) is subdominant, influencing only the long-term evolution of the particle distribution function, but not significantly affecting the dynamics on the much shorter time scale of the turbulent fluctuations. The ballistic term, the second term on the left-hand side of (2.1), describes the free streaming of particles along the direction parallel to magnetic field, and can lead to linear phase mixing of fluctuations in the particle density along this direction. The Lorentz force term, the third term on the left-hand side of (2.1), dictates the reaction of the charged plasma particles in response to the (self-consistently determined) electric and magnetic fields in the plasma, and therefore is the term that governs wave–particle interactions in a kinetic plasma.

The Lorentz force term, however, not only is responsible for the secular transfer of energy from the electromagnetic fields to the plasma particles that occurs when electromagnetic fluctuations are collisionlessly damped, but also describes the typical oscillatory transfer of energy between fields and particles that is characteristic of wave motion. The difficulty in identifying the collisionless damping of turbulent fluctuations in a kinetic plasma is that the oscillatory transfer of energy often has a much larger magnitude than the secular transfer of energy. For clarity, we define the oscillating energy transfer as the conservative transfer of energy back and forth between fields and particles that is typical of undamped linear wave motion in a kinetic plasma. We define the secular energy transfer as the energy lost from the electromagnetic fluctuations to the plasma particles through collisionless damping.

The Alfvén wave ideally illustrates the difference between the oscillating and secular energy transfer. Alfvén waves behave like waves on a stretched rubber band, where magnetic tension provides the restoring force and the kinetic energy of the transverse plasma motion gives rise to the inertia necessary to support wave motion. In an undamped Alfvén wave – for example, an Alfvén wave in the ideal magnetohydrodynamic (MHD) limit – energy is transferred back and forth between magnetic energy and kinetic energy conservatively, so the ideal MHD Alfvén wave has oscillating energy transfer but no secular energy transfer. In a kinetic treatment of the Alfvén wave in a weakly collisional plasma (Kulsrud 1983; Howes *et al.* 2006), resonant interactions between the electromagnetic wave and the particles propagating at velocities very near the phase velocity of the wave (the resonant particles) will lead to a net transfer of energy from the electromagnetic waves to the microscopic kinetic energy of the particles. For scales much larger than the ion Larmor radius, these resonant wave–particle interactions lead to weak but non-zero collisionless damping of the Alfvén wave, so the non-zero secular energy transfer is small relative to the oscillating energy transfer. For smaller scales at or below the ion Larmor

https://doi.org/10.1017/S0022377816001197 Published online by Cambridge University Press

radius, the Alfvén wave transitions to a kinetic Alfvén wave, and the collisionless damping by transit-time damping or Landau damping may become strong, leading to a significantly larger secular component of energy transfer relative to the oscillating component.

The primary aim of this paper is to distinguish the physics leading to the secular energy transfer from that governing the oscillating energy transfer and to exploit that insight to devise a method to determine the secular energy transfer from single-point measurements in a plasma. Furthermore, we highlight the characteristic signature in velocity space of this secular energy transfer via collisionless wave–particle interactions.

3. Theory of energy transfer in a Vlasov–Poisson plasma

The main goal of this study is to identify the secular transfer of energy from the electrostatic field to the particles via resonant collisionless wave–particle interactions, and to determine the impact of this resonantly transferred energy on the particle distribution functions. This theoretical insight will be used to devise a novel analysis strategy using correlated field and particle measurements to identify definitively the action of collisionless wave–particle interactions in heliospheric plasmas using either spacecraft measurements or nonlinear kinetic numerical simulations.

Here we review the properties of electrostatic fluctuations in a collisionless, unmagnetized plasma that are relevant to the aim of identifying the secular energy transfer via collisionless wave–particle interactions. For simplicity in the analytical calculations presented here, we consider a strictly one-dimensional (1D-1V) kinetic system, but we do note that the physics of electrostatic fluctuations ($\boldsymbol{\nabla} \times \boldsymbol{E} = 0$) remains unchanged in a realistic three-dimensional plasma. The dynamics of the electrostatic fluctuations in a collisionless 1D-1V plasma is governed by the Vlasov–Poisson equations, where the Vlasov equation determines the collisionless evolution of the distribution function for each species s, $f_s(x, v, t)$, given by

$$\frac{\partial f_s}{\partial t} + v\frac{\partial f_s}{\partial x} - \frac{q_s}{m_s}\frac{\partial \phi}{\partial x}\frac{\partial f_s}{\partial v} = 0 \tag{3.1}$$

and the Poisson equation yields the scalar electrostatic potential, $\phi(x, t)$,

$$\frac{\partial^2 \phi}{\partial x^2} = -4\pi \sum_s \int_{-\infty}^{+\infty} \mathrm{d}v\, q_s f_s. \tag{3.2}$$

Physically, the second term of the Vlasov equation describes the ballistic behaviour of the particles in the collisionless plasma and the third term governs the response of the particles to the electric field $E = -\partial\phi/\partial x$. Here we denote these terms the ballistic term and the wave–particle interaction term, respectively.

3.1. *Energy conservation*

To derive the expression for the conserved energy of electrostatic fluctuations in an unmagnetized plasma, we begin with the electrostatic analogue of Poynting's theorem. Beginning with the 1-D electrostatic limit of the Ampere–Maxwell Law, $\partial E/\partial t = -4\pi j$, we multiply by E to obtain the rate of change of electrostatic field energy density,

$$\frac{\partial}{\partial t}\left(\frac{E^2}{8\pi}\right) = -jE. \tag{3.3}$$

https://doi.org/10.1017/S0022377816001197 Published online by Cambridge University Press

Next, we multiply the Vlasov equation (3.1) for species s by $m_s v^2/2$ and integrate over velocity and position. Exchanging the order of differentiation and integration of the independent variables, we may obtain the form

$$\frac{\partial}{\partial t}\int \mathrm{d}x \int \mathrm{d}v \frac{1}{2} m_s v^2 f_s + \int \mathrm{d}x \frac{\partial}{\partial x}\left[\int \mathrm{d}v \frac{1}{2} m_s v^3 f_s\right] - \int \mathrm{d}x \frac{\partial \phi}{\partial x}\int \mathrm{d}v \left(\frac{q_s v^2}{2}\right)\frac{\partial f_s}{\partial v} = 0. \tag{3.4}$$

The first term of this equation represents the rate of change of the microscopic kinetic energy of species s

$$W_s \equiv \int_{-L/2}^{L/2} \mathrm{d}x \int_{-\infty}^{\infty} \mathrm{d}v \frac{1}{2} m_s v^2 f_s. \tag{3.5}$$

The second term, associated with the ballistic behaviour of particles, is a perfect differential in x, yielding zero for either periodic boundary conditions, $f_s(x = -L/2, v) = f_s(x = L/2, v)$, or boundary conditions at infinity, $\lim_{L\to\infty} f_s(x = \pm L/2, v) = 0$. Physically, the ballistic term can only transport energy from one position to another, so when integrated over the volume yields a net change of zero for W_s. The third term may be integrated by parts in velocity to yield the result

$$\frac{\partial W_s}{\partial t} = -\int \mathrm{d}x \frac{\partial \phi}{\partial x}\int \mathrm{d}v\, q_s v f_s = \int \mathrm{d}x\, j_s E, \tag{3.6}$$

where the current density for species s is given by $j_s = \int \mathrm{d}v\, q_s v f_s$.

Since the total current density $j = \sum_s j_s$, we may integrate (3.3) over space and combine it with (3.6) summed over species to obtain an expression for the conservation of energy in a 1D-1V electrostatic plasma,

$$\frac{\partial}{\partial t}\int \mathrm{d}x \left(\frac{E^2}{8\pi}\right) + \frac{\partial}{\partial t}\sum_s \int \mathrm{d}x \int \mathrm{d}v \frac{1}{2} m_s v^2 f_s = 0. \tag{3.7}$$

Therefore, the conserved Vlasov–Poisson energy W for electrostatic fluctuations in a collisionless, unmagnetized plasma is given by

$$W = \int \mathrm{d}x \frac{E^2}{8\pi} + \sum_s \int \mathrm{d}x \int \mathrm{d}v \frac{1}{2} m_s v^2 f_s. \tag{3.8}$$

We also define the electrostatic field

$$W_\phi \equiv \int \mathrm{d}x \frac{E^2}{8\pi}, \tag{3.9}$$

such that the total conserved Vlasov–Poisson energy for a single ion species plasma is given by

$$W = W_\phi + W_i + W_e. \tag{3.10}$$

https://doi.org/10.1017/S0022377816001197 Published online by Cambridge University Press

3.2. *Energy transfer via collisionless wave–particle interactions*

To illuminate the secular transfer of energy between the electrostatic field and the particles via resonant wave–particle interactions, it is instructive to examine more closely the different contributions to the change in the particle energy, W_s. As (3.7) mandates, in the Vlasov–Poisson system, the energy gain by the particles must be equal to the energy lost from the electrostatic field, $\sum_s \partial W_s/\partial t = -\partial W_\phi/\partial t$. We may express the rate of energy exchange (gain or loss) for species s by

$$\frac{\partial W_s}{\partial t} = \int \mathrm{d}x \int \mathrm{d}v \frac{1}{2} m_s v^2 \frac{\partial f_s}{\partial t}. \tag{3.11}$$

To progress further, we decompose the distribution function into an equilibrium and perturbed component,

$$f_s(x, v, t) = f_{s0}(v) + \delta f_s(x, v, t), \tag{3.12}$$

where the equilibrium distribution function $f_{s0}(v)$ is assumed to be uniform in space and static in time. We also make the additional assumption that $f_{s0}(v)$ is an even function of velocity so that the equilibrium has no bulk plasma flow (first moment), but it need not be a Maxwellian. Not that for solar wind measurements, we may transform to the frame of reference flowing with the solar wind plasma (see § 7.1 for more discussion of the frame of reference of measurements).

We emphasize here that we have made no ordering assumptions on the magnitude of δf_s relative to f_{s0}, so the nonlinear evolution of the distribution function described by this form is not limited in any way. The term δf_s contains the entire (nonlinear) perturbation, not just the lowest-order (linear) perturbation. Of course, the physical limitation

$$f_s(x, v, t) = f_{s0}(v) + \delta f_s(x, v, t) \geqslant 0 \tag{3.13}$$

must always be satisfied, so this means that $\delta f_s(x, v, t) \geqslant -f_{s0}(v)$ for all values of velocity v. Practically, this does lead to constraints on the allowable time step in numerical simulations to maintain a physically realizable $f_s(x, v, t) \geqslant 0$ everywhere.

Substituting (3.12) into the Vlasov equation (3.1), we obtain

$$\frac{\partial \delta f_s}{\partial t} = -v \frac{\partial \delta f_s}{\partial x} + \frac{q_s}{m_s} \frac{\partial \phi}{\partial x} \frac{\partial f_{s0}}{\partial v} + \frac{q_s}{m_s} \frac{\partial \phi}{\partial x} \frac{\partial \delta f_s}{\partial v}. \tag{3.14}$$

In this form, on the right-hand side, the first term is the (linear) ballistic term, the second term is the linear wave–particle interaction term and the third term is the nonlinear wave–particle interaction term. Next, we substitute (3.14) into (3.11), yielding

$$\frac{\partial W_s}{\partial t} = \int \mathrm{d}x \int \mathrm{d}v \frac{1}{2} m_s v^2 \left[-v \frac{\partial \delta f_s}{\partial x} + \frac{q_s}{m_s} \frac{\partial \phi}{\partial x} \frac{\partial f_{s0}}{\partial v} + \frac{q_s}{m_s} \frac{\partial \phi}{\partial x} \frac{\partial \delta f_s}{\partial v} \right]. \tag{3.15}$$

We now evaluate the influence of each of these terms on the evolution of the microscopic kinetic energy, W_s.

The first term, the ballistic term, may be written as a perfect differential in x, thereby yielding a value of zero upon integration over x for periodic or infinite

https://doi.org/10.1017/S0022377816001197 Published online by Cambridge University Press

boundaries. The second term, the linear wave–particle interaction term, may be written in the form

$$\int \mathrm{d}x \frac{\partial}{\partial x}\left\{\frac{q_s\phi}{2}\left[\int \mathrm{d}v v^2 \frac{\partial f_{s0}}{\partial v}\right]\right\} = 0. \tag{3.16}$$

Since we have chosen f_{s0} to be an even function of v, then its derivative $\partial f_{s0}/\partial v$ is an odd function, so the integrand of the velocity integral is an odd function evaluated over an even interval, yielding zero. In addition, because f_{s0} is not a function of x, everything in the braces is also a perfect differential, so this term will vanish upon integration over x for any choice of f_{s0}, not just even functions of v.

For the third term, the nonlinear wave–particle interaction term, we may integrate by parts in velocity to yield the final result for the rate of change of microscopic kinetic energy for species s,

$$\frac{\partial W_s}{\partial t} = -\int \mathrm{d}x \frac{\partial \phi}{\partial x}\int \mathrm{d}v q_s v \delta f_s = \int \mathrm{d}x j_s E. \tag{3.17}$$

Therefore, the secular change of particle energy in the Vlasov–Poisson system occurs via the nonlinear wave–particle interaction term in (3.14). Furthermore, the perturbations in the distribution function arising from the collisionless transfer of energy from fields to particles are generated by this term, making it possible to separate the fluctuations in velocity space due to resonant wave–particle interactions from the (generally larger-amplitude) fluctuations generated by the ballistic term and the linear wave–particle interaction term.

Note that linearization of the kinetic system leads to dropping the nonlinear wave–particle interaction term, the third term on the right-hand side of (3.15). But this term is necessary to describe the change in the energy of the particles W_s. So, although a linearized system will describe the collisionless Landau damping of the electrostatic waves of the Vlasov–Poisson system (Landau 1946), the Vlasov–Poisson energy W given by (3.8) is not conserved in a linearized system. The nonlinear wave–particle interaction term must be retained in order to achieve conservation of W, or an alternative Kruskal–Obermann energy (Kruskal & Oberman 1958; Morrison 1994) can be devised to achieve a conserved quadratic invariant of the linearized system.

In summary, using measurements of the fluctuations in the particle distribution function $\delta f_s(x, v, t)$ and the electric field $E(x, t)$, we may calculate the rate of transfer of energy from the fields to the particles by either form of the following expression,

$$\frac{\partial W_s}{\partial t} = -\int \mathrm{d}x \int \mathrm{d}v q_s \frac{v^2}{2}\frac{\partial \delta f_s(x, v, t)}{\partial v} E(x, t) = \int \mathrm{d}x \int \mathrm{d}v\, q_s v \delta f_s(x, v, t) E(x, t). \tag{3.18}$$

3.3. *Diagnosing secular energy transfer*

The key challenge in diagnosing the collisionless damping of fluctuations in a turbulent plasma is to separate the often small-amplitude signal of the secular energy transfer from the generally much larger-amplitude signal of the oscillating energy transfer. The arguments of the preceding section suggest that by integrating over all space – or taking a spatial average, as is done in quasilinear theory – we can average out the zero net effect of the oscillating energy transfer and extract the smaller secular energy transfer that is associated with collisionless damping. In this case, the spatial

https://doi.org/10.1017/S0022377816001197 Published online by Cambridge University Press

integration eliminates the contribution from the ballistic and linear wave–particle interaction terms in (3.14), isolating the non-zero net effect of the secular energy transfer due to the nonlinear wave–particle interaction term.

Of course, in a numerical simulation, where all of the spatial information is known, spatial integration can be used to isolate the secular energy transfer. But such spatial information is not accessible observationally, where spacecraft measurements are typically made at only a single point (or at most, a few points) in space. Furthermore, numerical simulations of plasma turbulence provide strong evidence that energy dissipation is often highly localized in space (Wan *et al.* 2012; Karimabadi *et al.* 2013; TenBarge & Howes 2013; Wu *et al.* 2013; Zhdankin *et al.* 2013; Zhdankin, Uzdensky & Boldyrev 2015*b*); so, even in numerical simulations, integration over a volume larger than the region of strong dissipation may obscure the details of the local dissipation mechanism, making it more difficult to identify the physical mechanism responsible. Here we aim to develop a method that can be used to analyse the secular energy transfer using single-point measurements of the electromagnetic fields and velocity distribution functions, enabling an improved analysis of the collisionless damping of turbulent fluctuations in both spacecraft measurements and kinetic numerical simulations.

Let us define the phase-space energy density for a particle species s by $w_s(x, v, t) = m_s v^2 f_s(x, v, t)/2$. Note that, for the 1D-1V Vlasov–Poisson system, this is the energy density per unit length per unit velocity. The integral of $w_s(x, v, t)$ over all velocity yields the spatial energy density of the plasma species as a function of position, which is the usual meaning of the term energy density. Subsequent integration over the spatial volume yields the total microscopic kinetic energy of the species, W_s.

If we want to understand how the phase-space energy density evolves in time, we can take the time derivative of $w_s(x, v, t)$ and replace $\partial f_s/\partial t$ using the Vlasov equation to obtain an expression for the instantaneous change of the phase-space energy density,

$$\frac{\partial w_s(x, v, t)}{\partial t} = -\frac{1}{2} m_s v^3 \frac{\partial \delta f_s}{\partial x} - q_s \frac{v^2}{2} \frac{\partial f_{s0}(v)}{\partial v} E(x, t) - q_s \frac{v^2}{2} \frac{\partial \delta f_s(x, v, t)}{\partial v} E(x, t). \quad (3.19)$$

From the analysis of the energy conservation equation (3.15), we know that, if this equation is integrated over all velocity and all physical space, only the third term contributes to the secular energy transfer from fields to particles (or *vice versa*). However, in the absence of these integrations, all three terms contribute to the instantaneous phase-space energy density change at each point in (x, v) phase space.

3.4. *Field–particle correlations*

The form of the term responsible for the secular energy transfer in (3.19) suggests that the product of $(-q_s v^2/2)(\partial \delta f_s(x, v, t)/\partial v)$ and $E(x, t)$ provides a direct measure of the rate of energy transfer (possibly including an oscillating component). To isolate the small secular component, we take the unnormalized field–particle correlation, $C_\tau(-q_s v^2/2 \partial \delta f_s/\partial v, E)$, at a single point in space over a selected correlation interval τ. By correlating the two signals over a sufficiently long interval (more than a linear wave period, $\tau \gtrsim 2\pi\omega$), the oscillating energy transfer is averaged out, extracting the smaller signal of the secular energy transfer.

For measurements of the velocity distribution and the electric field at a single point in space, $x = x_0$, this correlation is a function of velocity, time and the correlation

https://doi.org/10.1017/S0022377816001197 Published online by Cambridge University Press

interval,

$$C_E(v, t, \tau) = C_\tau \left(-q_s \frac{v^2}{2} \frac{\partial \delta f_s(x_0, v, t)}{\partial v}, E(x_0, t) \right). \tag{3.20}$$

Therefore, the general idea of diagnosing the energy transfer at each point in (x, v) phase space reduces, due to the observational constraints of single-point measurements, to the case of determining the distribution of the energy transfer rate in velocity space. A key advance with this method is that determining how the secular energy transfer rate varies in velocity space provides valuable new information about the physical mechanism responsible for the collisionless damping of the fluctuations. Different mechanisms, such as Landau damping or stochastic ion heating, are likely to have distinct signatures of this damping in velocity space. In this paper, we illustrate this field–particle correlation analysis method using the case of the Landau damping of Langmuir waves in a 1D-1V Vlasov–Poisson plasma, but the concept of using field–particle correlations to diagnose collisionless energy transfer is extremely general, and it can be also applied to examine the damping of turbulence in heliospheric plasmas using single-point spacecraft measurements.

There are two issues that merit further discussion regarding the construction of field–particle correlations. First, because the product of the two terms that are correlated is a direct measure of the instantaneous collisionless energy transfer (specifically, just the component due to the nonlinear wave–particle interaction term), the field–particle correlation is to be performed in the following way: (i) the mean values of the two correlated variables are not subtracted before multiplication; and (ii) the correlation is not normalized by the variances of each of the correlated variables. Although a normalized correlation can be performed and indeed contains information about the nature of the collisionless wave–particle interactions, the process of normalization effectively removes the amplitude variation of the energy transfer rate as a function of velocity, a vital piece of information provided by this analysis. A simple model that predicts the form of the normalized correlation for an exact linear eigenfunction in terms of the normalized damping rate $-\gamma/\omega$ is presented in appendix B.

The second issue regards the applicability of the particular field–particle correlation given in (3.20) to spacecraft observations. The often low velocity-space resolution of particle measurements by spacecraft instrumentation and the corruption by noise for low particle count rates mean that accurate computation of the necessary derivative $\partial \delta f_s(x, v, t)/\partial v$ may be difficult, or even impossible. But, as shown in § 3.2, upon integration over velocity space, both $(-q_s v^2/2)(\partial \delta f_s(x, v, t)/\partial v)$ and $q_s v \delta f_s(x, v, t)$ yield the same result for the total species current, $j_s(x, t)$. Therefore, we propose an alternative field–particle correlation

$$C'_E(v, t, \tau) = C_\tau(q_s v \delta f_s(x_0, v, t), E(x_0, t)) \tag{3.21}$$

that may be more suitable for implementation with low resolution spacecraft measurements of particle velocity distribution functions. Different collisionless damping mechanisms are likely to produce distinct signatures of any chosen form of field–particle correlation in velocity space. So, although the form $q_s v \delta f_s(x, v, t) E(x, t)$ does not correspond directly to the energy transfer rate at a point in (x, v) phase space as given by (3.19), this alternative field–particle correlation may still be valuable in distinguishing one collisionless damping process from another.

https://doi.org/10.1017/S0022377816001197 Published online by Cambridge University Press

4. Code description

Here we describe the nonlinear Vlasov–Poisson simulation code VP. Our approach is designed to highlight the perturbations to the distribution function f_s associated with secular transfer of energy from the electrostatic field to the plasma particles via collisionless wave–particle interactions. Since the distribution function $f_s(x, v, t) = f_{s0}(v) + \delta f_s(x, v, t)$ only appears linearly in the Vlasov equation, we may separate the evolution of different components of the perturbed distribution function,

$$\delta f_s = \delta f_{sB} + \delta f_{sWl} + \delta f_{sWn}, \tag{4.1}$$

denoted the (linear) ballistic term δf_{sB}, the linear wave term δf_{sWl} and the nonlinear wave term δf_{sWn}. The time evolution of these different terms is given by

$$\frac{\partial \delta f_{sB}}{\partial t} = -v \frac{\partial \delta f_s}{\partial x} \tag{4.2}$$

$$\frac{\partial \delta f_{sWl}}{\partial t} = \frac{q_s}{m_s} \frac{\partial \phi}{\partial x} \frac{\partial f_{s0}}{\partial v} \tag{4.3}$$

$$\frac{\partial \delta f_{sWn}}{\partial t} = \frac{q_s}{m_s} \frac{\partial \phi}{\partial x} \frac{\partial \delta f_s}{\partial v}. \tag{4.4}$$

As we shall see, the perturbed distribution function δf_s at a single point in space is dominated by the ballistic and linear wave terms, but it is the much smaller nonlinear wave term that represents the secular transfer of energy from fields to particles via collisionless wave–particle interactions. The motivation for this paper is to identify a strategy for isolating the much smaller perturbations associated with collisionless damping of the electrostatic field, so separating these different contributions helps to illuminate the different contributions to the collisionless energy transfer via wave–particle interactions.

The details of the numerical implementation used to evolve the separated components of the Vlasov equation, given by (4.2)–(4.4), and the calculation of the electrostatic potential, given by (3.2), are presented in appendix A. In addition, validation of the VP code by reproducing the results of the complex linear dispersion relation for Langmuir waves is presented in § A.2.

5. Evolution of the distribution function

In this section, we use the nonlinear Vlasov–Poisson simulation code VP to explore the secular energy transfer from the electrostatic field energy W_ϕ to particle microscopic kinetic energy W_s due to the Landau damping of Langmuir waves in a 1D-1V Vlasov–Poisson plasma. In particular, we focus on the perturbations of the particle velocity distribution functions arising as a consequence of this secular energy transfer. Three cases are used to illustrate the physics of the collisionless energy transfer: (I) a moderately damped case of a standing Langmuir wave pattern with $k\lambda_{de} = 0.5$; (II) a weakly damped case of a standing Langmuir wave pattern with $k\lambda_{de} = 0.25$; and (III) a moderately damped case of a single propagating Langmuir wave mode with $k\lambda_{de} = 0.5$. All cases have plasma parameters $T_i/T_e = 1$ and $m_i/m_e = 100$ and numerical resolution $n_x = 128$ and $n_v = 256$ in a simulation domain of length $L = 2\pi/k$. For the Landau damping of Langmuir waves in a plasma with $m_i/m_e = 100$, little of the electrostatic field energy is transferred collisionlessly to the ions, so we focus strictly on the evolution of the electron distribution function

https://doi.org/10.1017/S0022377816001197 Published online by Cambridge University Press

Quantity	Case I	Case II	Case III
Wavenumber, $k\lambda_{de}$	0.5	0.25	0.5
Density fluctuation, $\delta n_e/n_0$	0.1	0.025	0.07425
Potential amplitude, $-q_e\phi/T_e$	0.4	0.4	0.297
Domain size, L/λ_{de}	4π	8π	4π
Linear frequency, ω/ω_{pe}	1.43	1.11	1.43
Linear damping rate, $-\gamma/\omega_{pe}$	0.159	0.00203	0.159
Resonant velocity, $\omega/(kv_{te})$	2.86	4.4	2.86
Linear wave period, $\omega_{pe}T$	4.39	5.66	4.39
Nonlinear time, $\tau_{nl}\omega_{pe} = [(-q_e\phi/T_e)k^2\lambda_{de}^2]^{-1/2}$	3.16	4.00	3.67

TABLE 1. Langmuir wave damping simulation parameters. The collisionless damping rate is expected to deviate from the linear value due to the quasilinear evolution of the distribution function for times much longer than the nonlinear time (O'Neil 1965), $t \gg \tau_{nl}$.

$f_e(x,\ v,\ t)$. The fundamental parameters for these three simulations are presented in table 1. Note that the linear and nonlinear evolution of the Landau damping of Langmuir waves is well characterized in seminal works by O'Neil (1965) and Manfredi (1997).

5.1. *Case I: moderately damped standing Langmuir wave*

According to the procedure outlined in § A.1, we initialize a standing Langmuir wave pattern in VP with $k\lambda_{de} = 0.5$ using an electron density perturbation $\delta n_e/n_0 = 0.1$. For this wavenumber, a numerical solution of the linear dispersion relation for Langmuir waves gives $\omega/\omega_{pe} = 1.43$ and $\gamma/\omega_{pe} = -1.59 \times 10^{-1}$, yielding a resonant phase velocity $v_p/v_{te} = \omega/(kv_{te}) = 2.86$. For this simulation, $L = 4\pi\lambda_{de}$, $v_{max} = 5v_{te}$, and $f_{CFL} = 0.05$.

In figure 1, we plot the evolution of the perturbed energies of the system. The perturbed energy for a species s is given by

$$\delta W_s = \int_{-L/2}^{L/2} \mathrm{d}x \int_{-\infty}^{\infty} \mathrm{d}v \frac{1}{2} m_s v^2 \delta f_s, \tag{5.1}$$

where we include all contributions to the perturbation, $\delta f_s = \delta f_{sB} + \delta f_{sWl} + \delta f_{sWn}$. The total perturbed energy $\delta W = W_\phi + \delta W_i + \delta W_e$, with an initial value of $\delta W = 0.2453(n_0 T_e \lambda_{de}^3/2)$, is conserved to within 0.05 %. From figure 1, it is clear that the electrostatic electric field energy W_ϕ (green) is converted primarily to microscopic kinetic energy of the electrons δW_e (blue), with less than 0.2 % of the energy transferred to the ions δW_i (red). The normalized period of the standing Langmuir wave pattern with $k\lambda_{de} = 0.5$ is $\omega_{pe}T = 4.39$, so 99 % of the electrostatic energy in the wave pattern is secularly transferred to the electrons in approximately 3 periods.

Next we explore the different components of the perturbed electron distribution function for this nonlinear simulation at time $\omega_{pe}t = 19.64$ and position $x = 0$. Note that the position $x = 0$ is a maximum (anti-node) of the electric field standing wave pattern. In panel (*a*) of figure 2, we plot the total electron distribution function f_e (magenta), the equilibrium electron distribution function f_{e0} (black) and the total perturbed electron distribution function $\delta f_e = \delta f_{eB} + \delta f_{eWl} + \delta f_{eWn}$ (cyan). We can gain deeper insight into the nature of the fluctuations in the electron distribution function

https://doi.org/10.1017/S0022377816001197 Published online by Cambridge University Press

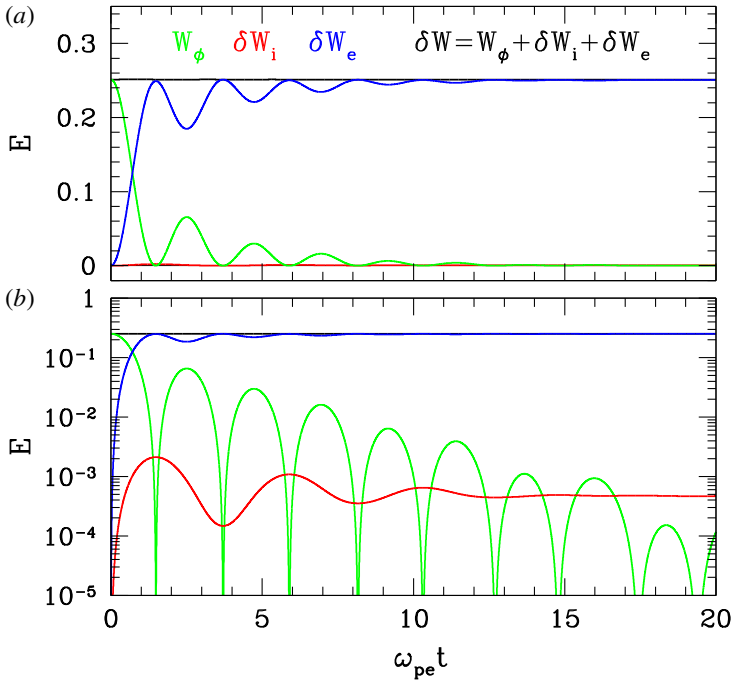

FIGURE 1. Energy evolution for the moderately damped Case I up to $\omega_{pe}t = 20$. Plotted are the total perturbed energy δW (black), field energy W_ϕ (green), perturbed ion energy δW_i (red) and perturbed electron energy δW_e (blue). Linear (*a*) and logarithmic (*b*) scales are both presented.

by separating out the components arising from the different terms in (3.14), shown in panel (*b*): (i) the ballistic term yields δf_{eB} (green), (ii) the linear wave–particle interaction term yields δf_{eWl} (blue) and (iii) the nonlinear wave–particle interaction term yields δf_{eWn} (red). As shown in § 3.2, it is only the nonlinear wave–particle interaction term that leads to a secular transfer of energy from the electrostatic field to the electrons, and this component of the perturbed electron distribution function is generally much smaller than the ballistic and linear wave–particle interaction components. The primary aim of this paper is to devise a procedure to isolate this small component of the fluctuations in the distribution function using only single-point measurements of the particle velocity distribution functions and the electrostatic field.

If full spatial information about the fluctuations is available, then a spatial average (or integration) over the volume eliminates the large fluctuations associated with the oscillatory energy transfer. This is the standard approach in quasilinear theory, taking a spatial average of the distribution function over the volume to obtain $\delta f_{eQL}(v, t) = (1/L) \int \mathrm{d}x\, \delta f_e(x, v, t)$. In panel (*a*) of figure 3, we plot the total electron distribution function evaluated at position $x = 0$, $f_e(0, v, t)$ (thin magenta) and the spatially averaged, quasilinear distribution function $f_{eQL}(v, t)$ (thick magenta) at time $\omega_{pe}t = 19.64$. It is clear that spatial average eliminates almost all of the fluctuations of the distribution function away from the equilibrium f_{e0} (black). To better see the deviations of the quasilinear distribution function from the equilibrium, in panel (*b*) we plot an expanded view of the nonlinear wave–particle interaction component of the perturbed electron distribution function at position $x = 0$, $\delta f_{eWn}(0, v, t)$ (thin

https://doi.org/10.1017/S0022377816001197 Published online by Cambridge University Press

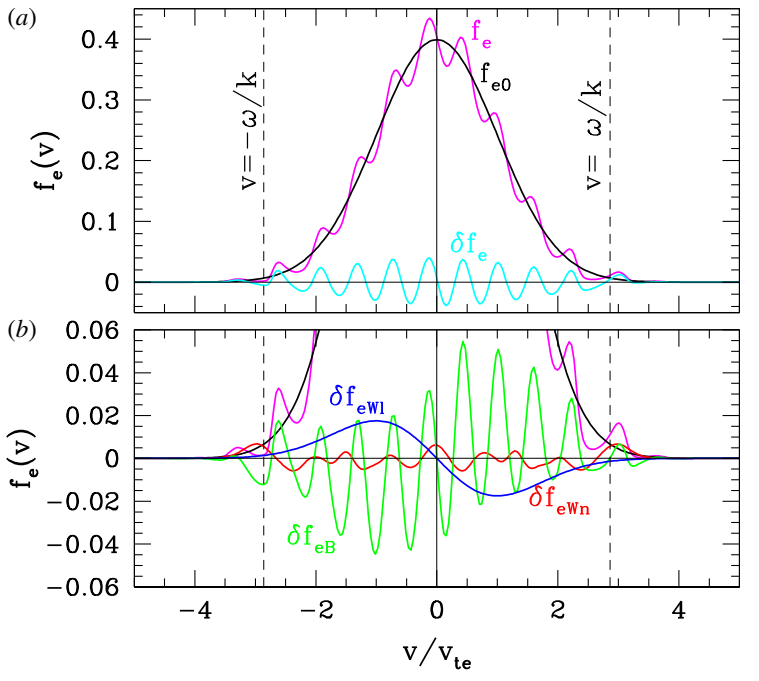

FIGURE 2. For Case I, (*a*) total electron distribution function f_e (magenta), equilibrium electron distribution function f_{e0} (black) and total perturbed electron distribution function δf_e (cyan). (*b*) The separated components of the perturbed electron distribution function: (i) δf_{eB} (green), (ii) δf_{eWl} (blue) and (iii) δf_{eWn} (red). Dashed vertical black lines denote the resonant velocities $v = \pm\omega/k$.

red) and the quasilinear perturbed distribution function $\delta f_{eQL}(v, t)$ (thick red). The total quasilinear distribution function $f_{eQL}(v, t)$ (thick magenta) in this bottom plot shows a quasilinear flattening of the distribution function at the resonant velocities $v = \pm\omega/k$, where the flattening occurs at both positive and negatives values of the Langmuir wave phase velocity because the standing wave pattern consists of equal-amplitude Langmuir waves propagating in opposite directions. Note that, when only single-point measurements at $x = 0$ are observed, the large perturbations of the distribution function associated with the oscillating energy transfer (due to the ballistic and linear wave–particle interaction terms) obscure this quasilinear flattening effect when the total electron distribution function evaluated at position $x = 0$, $f_e(0, v, t)$ (thin magenta), is plotted.

The key point of figure 3 is that the perturbed component of the electron distribution function due to the nonlinear wave–particle interaction term measured at a single point in space, δf_{eWn} (thin red), agrees closely with the spatially averaged, quasilinear perturbed distribution function $\delta f_{eQL}(v, t)$ (thick red). Thus, if we can devise a procedure to isolate the perturbation due to the nonlinear wave–particle interaction term from the larger fluctuations, shown in figure 2(*b*), then single-point measurements can be used to determine the secular energy transfer associated with the collisionless damping of the electrostatic Langmuir waves. We will show in § 6 that the correlation given by (3.20) can accomplish this isolation of the secular energy transfer.

Although the aim of this paper it is determine what insight can be gained from single-point measurements of the electromagnetic fields and particle velocity

https://doi.org/10.1017/S0022377816001197 Published online by Cambridge University Press

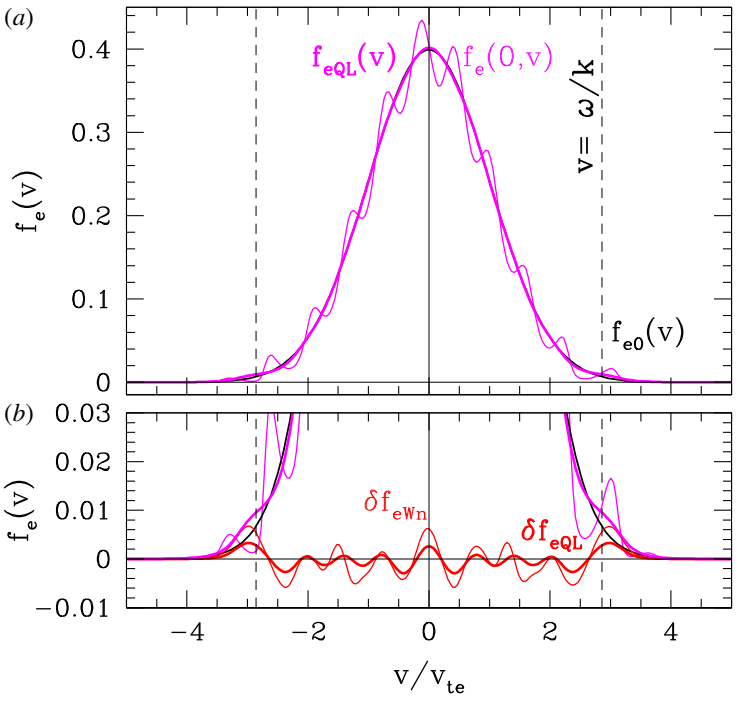

FIGURE 3. For Case I, (*a*) total electron distribution function evaluated at position $x = 0$, $f_e(0, v, t)$ (thin magenta), the spatially averaged, quasilinear distribution function $f_{eQL}(v, t)$ (thick magenta) and the equilibrium electron distribution function f_{e0} (black). (*b*) The nonlinear wave–particle interaction component of the perturbed electron distribution function at position $x = 0$, $\delta f_{eWn}(0, v, t)$ (thin red), the quasilinear perturbed distribution function $\delta f_{eQL}(v, t)$ (thick red). The quasilinear flattening of the distribution function at the resonant velocities $v = \pm\omega/k$ (dashed black) is apparent in the total quasilinear distribution function $f_{eQL}(v, t)$ (thick magenta), but this signature is obscured in the total electron distribution function evaluated at position $x = 0$, $f_e(0, v, t)$ (thin magenta).

distribution functions, it is instructive to examine how the different terms in the Vlasov equation contribute to the evolution of the distribution function throughout 1D-1V phase space. In figure 4, for Case I at $\omega_{pe}t = 19.64$, we plot on the full (x, v) phase space (*a*) the total perturbed electron distribution function δf_e, (*b*) the ballistic contribution δf_{eB}, (*c*) the linear wave contribution δf_{eWl} and (*d*) the nonlinear wave contribution δf_{eWn}. These plots demonstrate that it is quite difficult to see any features at the resonant velocities (green lines) in the total perturbed electron distribution function δf_e because, focusing on the amplitudes of each of these plots, the ballistic contribution δf_{eB} and linear wave contribution δf_{eWl} dominate the perturbation to the distribution function. Only the nonlinear wave term δf_{eWn} shows any obvious feature at the resonant velocities, generally showing an increase in particle energy just above the resonance at $|v| > |\omega/k|$ and a decrease just below the resonance at $|v| < |\omega/k|$, qualitatively consistent with the quasilinear flattening of the distribution function at the resonance. The full phase-space plot shows that the nonlinear wave term δf_{eWn} is not spatially uniform in x. In fact, the amplitude variation of the nonlinear perturbation in x reflects the amplitude variation of the electric field standing wave pattern in x: as noted in § A.1, the standing wave pattern is initialized with an electron

https://doi.org/10.1017/S0022377816001197 Published online by Cambridge University Press

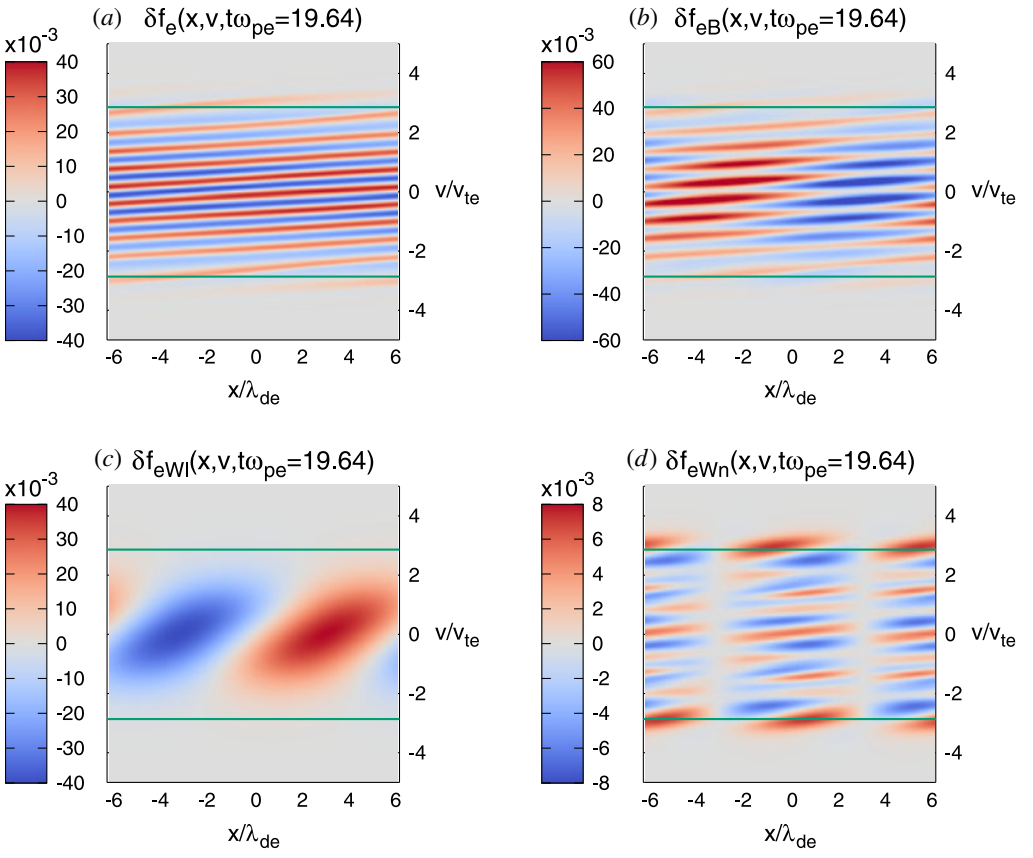

FIGURE 4. Plots of the full (x, v) phase space at time $\omega_{pe}t = 19.64$ for Case I, showing (a) the total perturbed electron distribution function f_e, (b) the ballistic contribution δf_{eB}, (c) the linear wave contribution δf_{eWl} and (d) the nonlinear wave contribution δf_{eWn}. Green horizontal lines indicate the resonant velocities.

density perturbation $\delta n_e \propto \sin(kx)$, leading to an electric field pattern $E \propto \cos(kx)$; the interaction of the standing electric field pattern leads to a pattern of the nonlinear wave term δf_{eWn} that is also modulated in amplitude by $\cos(kx)$, as evident in panel (d).

Also notable in these phase-space plots is absence of any strongly nonlinear features, such as trapping in phase-space vortices. These features do not arise because the perturbation amplitude is too small for such features to develop over the time scales simulated here (up to $\omega_{pe}t = 40$). As shown in figure 3, the evolution is indeed well described by the quasilinear average, further reinforcing that the nonlinear evolution is a higher-order (long-time) correction to the linear evolution. This is the appropriate regime for the intended application of this new field–particle correlation technique to heliospheric turbulence, such as the solar wind. In the solar wind, the magnetic field fluctuations at the ion kinetic length scales have typical amplitudes $\delta B/B \lesssim 0.1$; the fluctuations of the velocity distribution are expected to be approximately the same order of magnitude, $\delta f(v)/f_0(v) \sim \delta B/B \lesssim 0.1$, so the amplitudes chosen for the test case presented here are indeed relevant to the turbulent heliospheric plasmas of interest.

https://doi.org/10.1017/S0022377816001197 Published online by Cambridge University Press

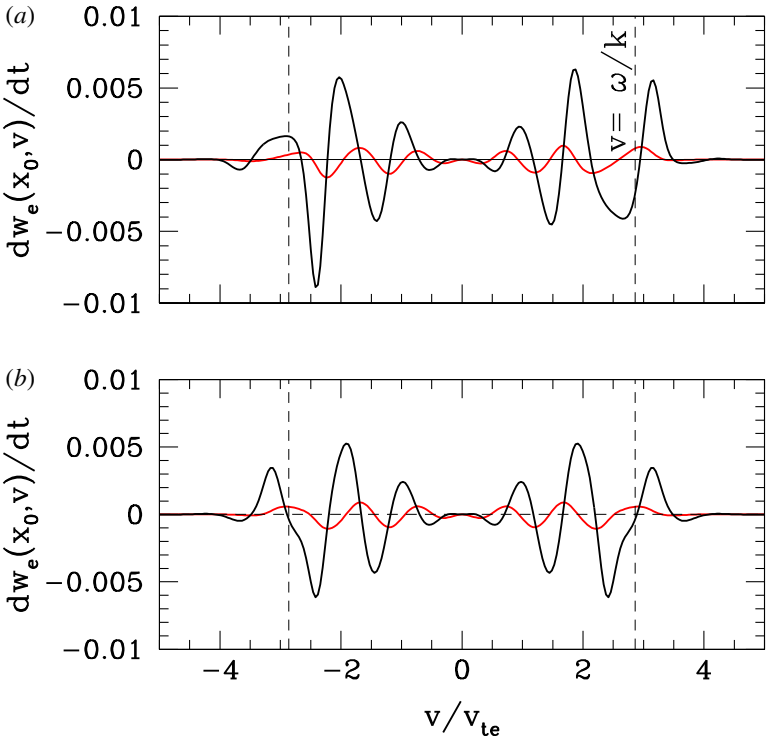

FIGURE 5. (*a*) Plot of $-q_e(v^2/2)\partial\delta f_e(x_0, v)/\partial v E(x_0)$ (black) and $q_e v\delta f_e(x_0, v)E(x_0)$ (red) evaluated at time $\omega_{pe}t = 11.29$ and position $x_0 = 0$. (*b*) Plot of the even (in v) components of the same curves in panel (*a*).

As a final note, we compare the product of the correlated quantities given in (3.20) and (3.21) as a function of the velocity. In figure 5(*a*), we plot $F(v) = -q_e(v^2/2)\partial\delta f_e(x_0, v)/\partial v E(x_0)$ (black) and $F'(v) = q_e v\delta f_e(x_0, v)E(x_0)$ (red) evaluated at time $\omega_{pe}t = 11.29$ and position $x_0 = 0$. Recall that the form $-q_e(v^2/2)\partial\delta f_e(x_0, v)/\partial v E(x_0)$ is direct computation of the rate of change of phase-space energy density due to the nonlinear particle interaction term in (3.19), and this is the only term that yields a non-zero secular energy transfer. When integrated over velocity, both of these forms yield the same rate of change of the spatial energy density at x_0 (since they are equivalent through an integration by parts in velocity). Although these two quantities indeed have very different structures as a function of velocity, they are indeed related. The zero crossings of $-q_e(v^2/2)\partial\delta f_e(x_0, v)/\partial v E(x_0)$ correspond closely (though not exactly*) with the minima and maxima of $q_e v\delta f_e(x_0, v)E(x_0)$. Thus, although the form given by the correlation (3.21) does not correspond directly to the rate of change of phase-space energy density, this more observationally accessible quantity can still provide valuable information about the distribution of the secular energy transfer from fields to particles as a function of the particle velocity.

*For a zero of $\partial\delta f_e/\partial v$ at v_0, the deviation Δv of the position of an extremum of $v\delta f_e$ from v_0 is given by $\Delta v/v_0 = \delta f_e(v_0)/(\delta f_e(v_0) - v_0^2\partial^2\delta f_e/\partial v^2)$ for $\Delta v/v_0 \ll 1$. For sufficiently oscillatory functions $\delta f_e(v)$, such as the examples shown in figure 5, this difference Δv scales as $(v/v_{te})^{-2}$, becoming increasingly small for $v > v_{te}$.

https://doi.org/10.1017/S0022377816001197 Published online by Cambridge University Press

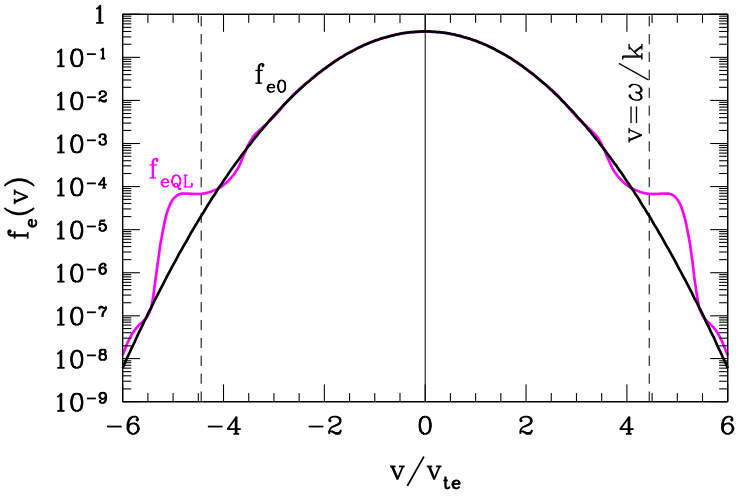

FIGURE 6. Quasilinear electron distribution function f_{eQL} (magenta) and equilibrium distribution function f_{e0} (black). Dashed vertical black lines denote the resonant velocities $v = \pm\omega/k$.

The correspondence between the two curves in figure 5(*a*) can be made a little more clear by taking just the component of these products that have an even parity in velocity, $F_{even}(v) = [F(v) + F(-v)]/2$. Because the odd component, $F_{odd}(v) = [F(v) - F(-v)]/2$, yields no net phase-space energy density change when integrated over velocity, plotting only the even component in panel (*b*) more clearly shows the variation of the energy transfer rate about the resonant velocity (dashed vertical black) – specifically, a loss of energy at $|v| < |\omega/k|$ and a gain of energy at $|v| > |\omega/k|$.

5.2. *Case II: weakly damped standing Langmuir wave*

We initialize a standing Langmuir wave pattern in VP, using the procedure outlined in § A.1, with $k\lambda_{de} = 0.25$ and an electron density perturbation $\delta n_e/n_0 = 0.025$, yielding an initial total perturbed energy of $\delta W = 0.1256(n_0 T_e \lambda_{de}^3/2)$. For this wavenumber, a numerical solution of the linear dispersion relation for Langmuir waves gives $\omega/\omega_{pe} = 1.11$ and $\gamma/\omega_{pe} = -2.03 \times 10^{-3}$, yielding a resonant phase velocity $v_p/v_{te} = \omega/(kv_{te}) = 4.4$. For this simulation, $L = 8\pi\lambda_{de}$, $v_{max} = 6v_{te}$, and $f_{CFL} = 0.05$.

In this simulation, the collisionless damping of the Langmuir wave is very weak because the resonant velocity occurs far out in the tail of the electron distribution function at $v_p/v_{te} = 4.4$, so there are few electrons to interact resonantly with the electric field fluctuations. Thus, it takes very little electrostatic field energy to flatten the electron distribution function at the resonant velocity, eliminating further Landau damping. We illustrate this in figure 6, where the total quasilinear electron distribution function f_{eQL} (magenta) is plotted at $\omega_{pe}t = 28.63$ along with the equilibrium distribution function f_{e0} (black). Here the value of the distribution function must be plotted logarithmically to see the perturbations to the distribution function, which occur at an amplitude four orders of magnitude smaller than the peak of the velocity distribution. This minute secular transfer of energy from the electric field to the electrons is likely to be unobservable given the instrumental noise levels for spacecraft particle measurements.

https://doi.org/10.1017/S0022377816001197 Published online by Cambridge University Press

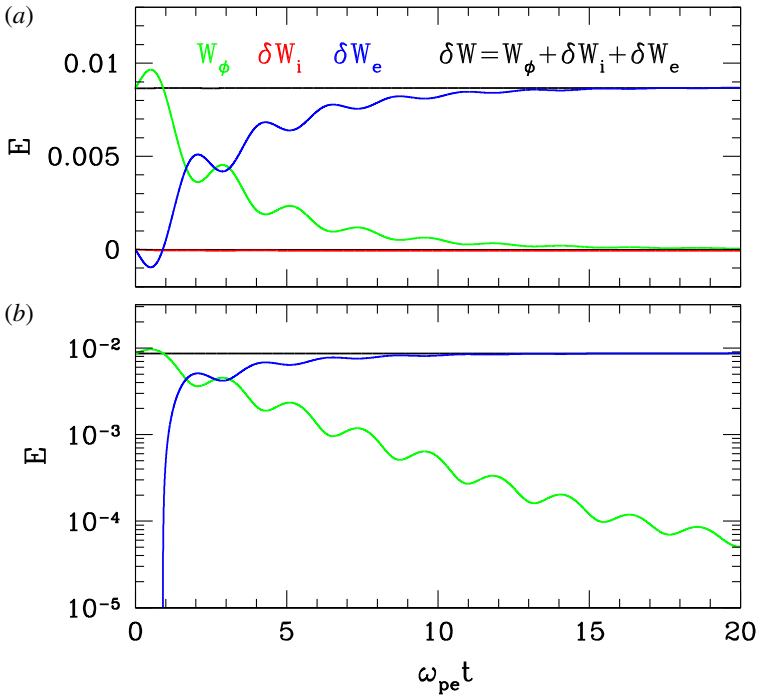

FIGURE 7. Energy evolution for the moderately damped single Langmuir wave with $k\lambda_{de} = 0.5$ up to $\omega_{pe}t = 20$. Plotted are the total perturbed energy δW (black), field energy W_ϕ (green), perturbed ion energy $\delta W_{\delta f_i}$ (red) and perturbed electron energy $\delta W_{\delta f_e}$ (blue). Linear (*a*) and logarithmic (*b*) scales are both presented.

5.3. *Case III: moderately damped single Langmuir wave mode*

In this simulation, a single Langmuir wave with $k\lambda_{de} = 0.5$ and amplitude $-q_e\phi_1/T_e = 0.297$ propagating in the $+x$ direction is initialized using the solution of the linear dispersion relation for the Langmuir wave mode, as detailed in § A.1. Both the electron and ion distribution functions are initialized according to (A 9) using the numerically determined complex frequency from a linear dispersion relation solver, $\omega/\omega_{pe} = 1.43$ and $\gamma/\omega_{pe} = -1.59 \times 10^{-1}$. To minimize transients in the simulation initialization, these initialized eigenfunctions are smoothed in velocity space using a Crank–Nicholson diffusion operator in velocity space $N_s = 15$ times with a diffusion coefficient $\nu/(\Delta v)^2 = 1.5625 \times 10^{-3}$. For this wave, the resonant phase velocity $v_p/v_{te} = \omega/(kv_{te}) = 2.86$. For this simulation, $L = 4\pi\lambda_{de}$, $v_{max} = 5v_{te}$, and $f_{CFL} = 0.05$.

In figure 7, we plot the evolution of the perturbed energies of the system. Total perturbed energy $\delta W = W_\phi + \delta W_i + \delta W_e$, with an initial value of $\delta W = 0.008659(n_0 T_e \lambda_{de}^3/2)$, is conserved to within 0.1 %. This figure shows that the electrostatic field energy W_ϕ (green) is converted primarily to microscopic kinetic energy of the electrons δW_e (blue).

For the evolution of this single Langmuir wave, we plot in figure 8 the perturbed electron distribution function for this nonlinear simulation at time $\omega_{pe}t = 19.64$ and position $x = 0$. In panel (*a*), we plot the total electron distribution function f_e (magenta), the equilibrium electron distribution function f_{e0} (black) and the total perturbed electron distribution function $\delta f_e = \delta f_{eB} + \delta f_{eWl} + \delta f_{eWn}$ (cyan). The separate

https://doi.org/10.1017/S0022377816001197 Published online by Cambridge University Press

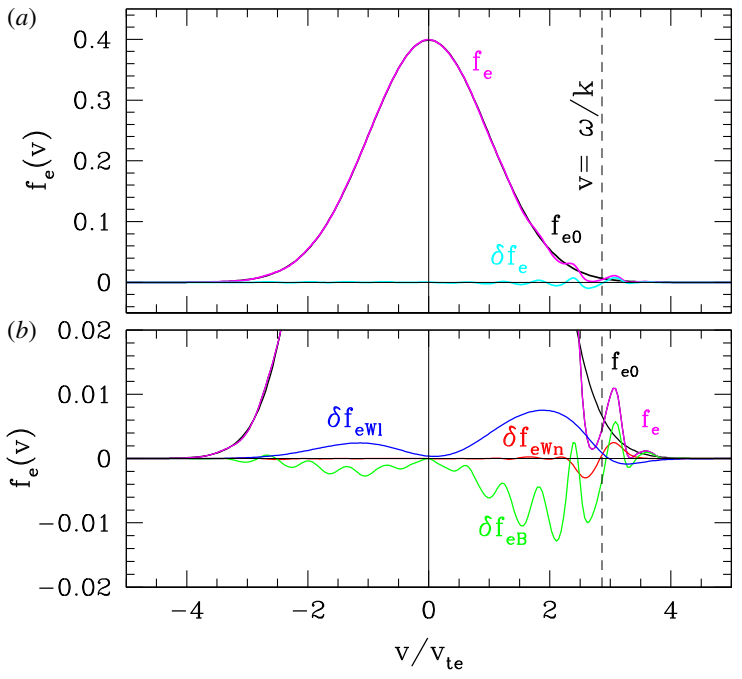

FIGURE 8. (*a*) Total electron distribution function f_e (magenta), equilibrium electron distribution function f_{e0} (black) and total perturbed electron distribution function δf_e (cyan). (*b*) The separated components of the perturbed electron distribution function: (i) δf_{eB} (green), (ii) δf_{eWl} (blue) and (iii) δf_{eWn} (red). The dashed vertical black line denotes the resonant velocity $v = \omega/k$.

components arising from the different terms in (3.14) are shown in panel (*b*): (i) the ballistic term yields δf_{eB} (green), (ii) the linear wave–particle interaction term yields δf_{eWl} (blue) and (iii) the nonlinear wave–particle interaction term yields δf_{eWn} (red). In this simulation, the perturbations of the distribution function are highly localized around the resonant velocity (dashed black). Again, as in the case of the Landau damping of the standing wave pattern, the perturbations due to the ballistic and linear wave–particle interaction terms are much larger than that due to the nonlinear wave–particle interaction term, making the isolation of this term a significant challenge.

In figure 9(*a*), we compare the spatially averaged, quasilinear distribution function $f_{eQL}(v,\ t)$ (thick magenta) at time $\omega_{pe}t = 19.64$ with the total electron distribution function evaluated at position $x = 0$, $f_e(0,\ v,\ t)$ (thin magenta). For the small amplitude of the initialized Langmuir wave, the deviation of $f_{eQL}(v,\ t)$ from the equilibrium f_{e0} (black) is difficult to see at this scale, so, in panel (*b*), we plot the total quasilinear distribution function $f_{eQL}(v, t)$ (thick magenta) and the equilibrium f_{e0} (black), showing the quasilinear flattening at the resonant velocity $v = \omega/k$ (dashed black). The total electron distribution function evaluated at position $x = 0$, $f_e(0,\ v,\ t)$ (thin magenta), has much larger fluctuations, dominated by the ballistic and linear wave–particle interaction terms, that obscure the signature of the quasilinear flattening. We also plot the perturbed distribution function $\delta f_{eQL}(v,\ t)$ (thick red) and the nonlinear wave–particle interaction component of the perturbed electron distribution function at position $x = 0$, $\delta f_{eWn}(0,\ v,\ t)$ (thin red) – these two curves coincide almost exactly in

https://doi.org/10.1017/S0022377816001197 Published online by Cambridge University Press

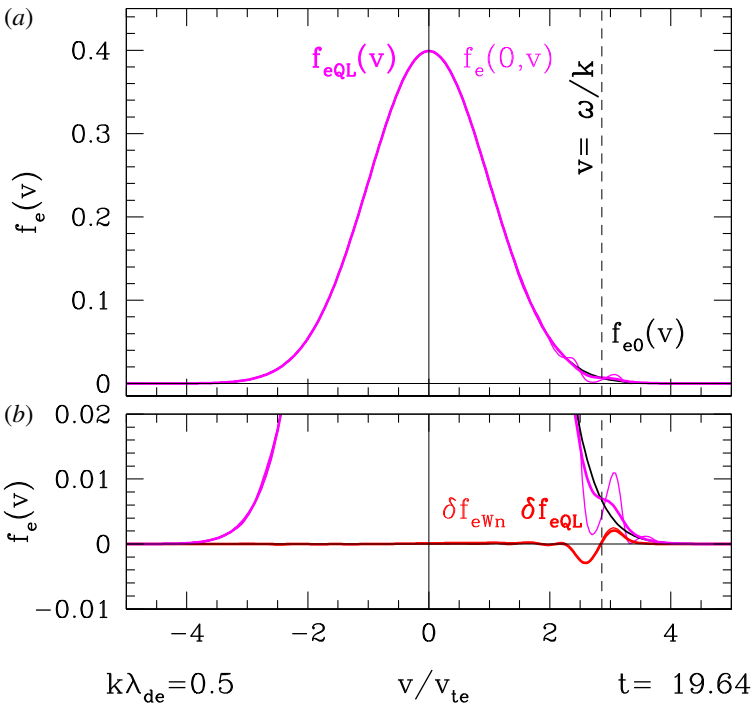

FIGURE 9. (*a*) Total electron distribution function evaluated at position $x = 0$, $f_e(0, v, t)$ (thin magenta), the spatially averaged, quasilinear distribution function $f_{eQL}(v, t)$ (thick magenta) and the equilibrium electron distribution function f_{e0} (black). (*b*) The nonlinear wave–particle interaction component of the perturbed electron distribution function at position $x = 0$, $\delta f_{eWn}(0, v, t)$ (thin red) and the quasilinear perturbed distribution function $\delta f_{eQL}(v, t)$ (thick red) coincide exactly here. The quasilinear flattening of the distribution function at the resonant velocity $v = \omega/k$ (dashed black) is apparent in the total quasilinear distribution function $f_{eQL}(v, t)$ (thick magenta).

this case, providing motivation that single-point measurements can indeed be used to determine the secular energy transfer from the electrostatic field to the electrons.

In figure 10, for Case III at $\omega_{pe}t = 19.64$, we plot on the full (x, v) phase space (*a*) the total perturbed electron distribution function f_e, (*b*) the ballistic contribution δf_{eB}, (*c*) the linear wave contribution δf_{eWl} and (*d*) the nonlinear wave contribution δf_{eWn}. Although all of these perturbations to the electron distribution functions only have significant amplitudes at positive velocities, concentrated somewhat around the resonant velocity (green line), only the nonlinear wave contribution δf_{eWn} is highly localized in velocity around the resonant velocity, with the characteristic qualitative signature of quasilinear damping (phase-space energy density loss at $v < \omega/k$ and gain at $v > \omega/k$). Note also that the effect of the resonant wave–particle interaction that transfer energy from the electric field to the electrons does not show the significant variation along x: the reason is that electric field associated with the propagating Langmuir wave travels across the domain, having crossed the domain more than four times by $\omega_{pe}t = 19.64$, leading to the energization of the electrons (at the expense of the electric field energy) being spread fairly evenly across x.

https://doi.org/10.1017/S0022377816001197 Published online by Cambridge University Press

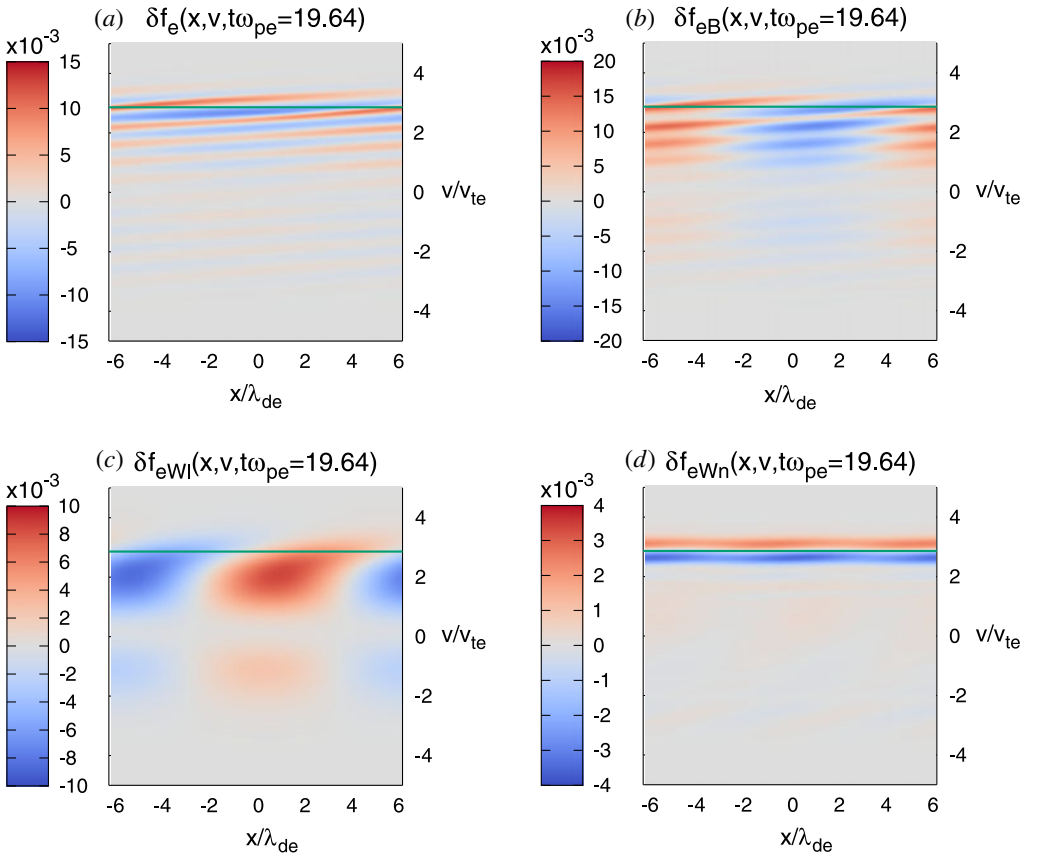

FIGURE 10. Plots of the full (x, v) phase space at time $\omega_{pe}t = 19.64$ for single Langmuir wave Case III, showing (a) the total perturbed electron distribution function f_e, (b) the ballistic contribution δf_{eB}, (c) the linear wave contribution δf_{eWl} and (d) the nonlinear wave contribution δf_{eWn}. The green horizontal line indicates the resonant velocity for this single propagating Langmuir wave.

6. Field–particle correlations

Here we define specifically how we compute the unnormalized correlation given in (3.20). Consider distribution function and electric field measurements at point $x = x_0$ measured at a time cadence of Δt. Labelling the discrete times of the measurements as $t_j \equiv t(j\Delta t)$ for $j = 0, 1, 2, \ldots$, we define $\delta f_{sj}(v) \equiv \delta f_s(x_0, v, t_j)$ and $E_j \equiv E(x_0, t_j)$. For a chosen correlation interval of $\tau = N\Delta t$, N points will be used for the correlation. With these definitions, the correlation at time $t = t_i$ is defined by

$$C_E(v, t_i, \tau) = \frac{1}{N} \sum_{j=i}^{i+N-1} q_s \frac{v^2}{2} \frac{\partial \delta f_{sj}(v)}{\partial v} E_j. \tag{6.1}$$

This procedure is essentially just a sliding time average of the rate of change of the phase-space energy density. The discrete velocity derivatives are computed using the same second-order, centred finite difference scheme described in appendix A. Note also that this scheme may be used even for a point of measurement moving with

https://doi.org/10.1017/S0022377816001197 Published online by Cambridge University Press

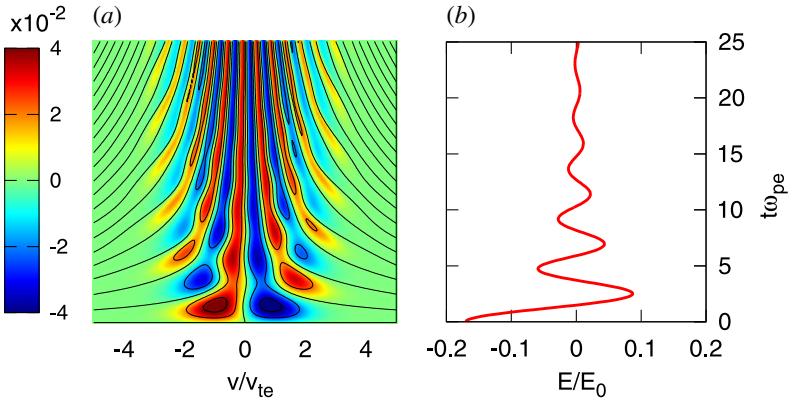

FIGURE 11. For Case I, (*a*) the total perturbed electron distribution function $\delta f_e(0, v, t)$ (colour map) and (*b*) electric field $E(0, t)$ measured at $x = 0$ as a function of normalized time $\omega_{pe}t$.

respect to the plasma by simply replacing $x_0 = x_0(t)$. We discuss implications using measurements made at a point in space moving with respect to the plasma below in § 7.1.

6.1. *Case I: moderately damped standing Langmuir wave*

Before presenting the results of the field–particle correlation technique applied to the problem of the collisionless damping of electrostatic Langmuir waves, we begin with a plot of the single-point measurements used for this analysis. For the case of the moderately damped standing Langmuir wave pattern presented in § 5.1, we plot in figure 11(*a*) the total perturbed electron distribution function $\delta f_e(0, v, t)$ (colour map) and (*b*) the electric field $E(0, t)$ measured at $x = 0$ as a function of normalized time $\omega_{pe}t$. Here the electric field is normalized to $E_0 = T_e/(q_e\lambda_{de})$. The data plotted in figure 11 correspond to observable quantities that can be derived from single-point spacecraft measurements.

In figure 12, we plot the products of the quantities used in the correlations $C_E(v, t, \tau)$ and $C'_E(v, t, \tau)$: (*a*) $(-q_e v^2/2)(\partial \delta f_e(0, v, t)/\partial v)E(0, t)$ and (*b*) $q_e v \delta f_e(0, v, t)$ $E(0, t)$ as a function of velocity v/v_{te} and time $\omega_{pe}t$. Note that the regions of velocity space where these functions have a significant amplitude are not especially well correlated with the resonant velocities (dot-dashed green). Without taking the correlation of these quantities over an appropriate correlation interval τ (typically one or more periods of a wave), the small-amplitude signal of the secular energy transfer is masked by the much larger-amplitude oscillating energy transfer, making it difficult to determine resonant nature of the collisionless damping.

A key part of this field–particle correlation analysis is the selection of an appropriate correlation interval τ to isolate successfully the small-amplitude secular energy transfer in the presence of a much larger-amplitude oscillating energy transfer. For this case, the standing wave period is $\omega_{pe}T = 4.39$. In figure 13(*a*,*b*), we plot the correlation $C_E(v_0, t, \tau)$ from (3.20) over a range of correlation intervals $0 \leqslant \omega_{pe}\tau \leqslant 16$ at two velocity values, (*a*) off-resonance at $v_0 = 0.08v_{te}$ and (*b*) on-resonance at $v_0 = 2.85v_{te}$. Note that the $\tau = 0$ curve (dark blue) corresponds to a vertical slice along figure 12(*a*) at the specified velocity v_0. The impact of increasing the correlation interval τ is

https://doi.org/10.1017/S0022377816001197 Published online by Cambridge University Press

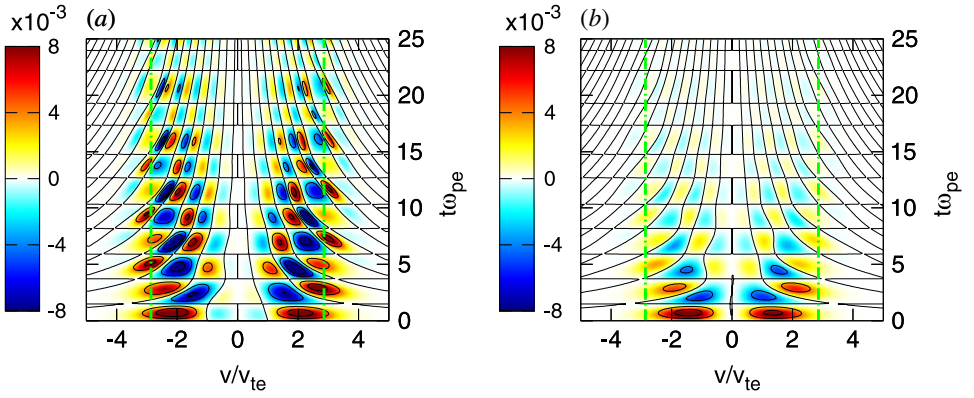

FIGURE 12. For Case I, plots of (a) the $C_E(v,\ t,\ \tau)$ correlation quantity, $(q_s v^2/2)(\partial \delta f_s(0,\ v,\ t)/\partial v)E(0,\ t)$ and (b) the $C'_E(v,\ t,\ \tau)$ correlation quantity, $q_s v \delta f_s(0,\ v,\ t)E(0,\ t)$, at $x = 0$ as a function of velocity v/v_{te} and time $\omega_{pe}t$. The dot-dashed vertical green lines denote the resonant velocities $v = \pm\omega/k$.

clear. As the correlation interval increases, the large-amplitude oscillations of the $\tau = 0$ case (blue), which are dominated by the oscillating energy transfer, are averaged out, isolating the smaller-amplitude secular energy transfer for correlation intervals longer than the wave period, $\tau > T$ (red). Note that the amplitude of the energy transfer rate – estimated by the correlation $C_E(v_0,\ t,\ \tau)$ – at $v_0 = 0.08v_{te}$ is two orders of magnitude smaller than at $v_0 = 2.85v_{te}$, so only the latter would likely be observable, given limitations to the sensitivities of particle instruments aboard spacecraft.

As shown in § 3, the correlation $C_E(v_0,\ t,\ \tau)$ in (3.20) is a direct calculation of the rate of energy transfer between the electrostatic field and the plasma particles. Therefore, to determine the accumulated energy transfer to the electrons, we can simply integrate this correlation over time. Thus, we obtain the total accumulated change in the electron phase-space energy density at $x = x_0$, $\Delta w_e(x_0,\ v,\ t)$, given by

$$\Delta w_e(x_0,\ v,\ t) = \int_0^t C_E(v,\ t',\ \tau)\,\mathrm{d}t'. \tag{6.2}$$

In figure 13(*c*,*d*), we plot the time-integrated correlation, giving the change in the electron phase-space energy density $\Delta w_e(x_0,\ v,\ t)$ as a function of time $\omega_{pe}t$ at the same two velocity values, (c) off-resonance at $v_0 = 0.08v_{te}$ and (d) on-resonance at $v_0 = 2.85v_{te}$. Note again that the change in phase-space energy density is several orders of magnitude larger for the resonant case at $v_0 = 2.85v_{te}$. The take away lesson here is that, by selecting a correlation interval $\tau \gtrsim 1.5T$, the large-amplitude oscillating energy transfer rate can be averaged out, isolating the signal of the secular energy transfer rate to the electrons associated with the collisionless damping of the electrostatic field.

Another point worth mentioning is that the total accumulated change in the electron phase-space energy density, Δw_e, decreases as the correlation interval is increased in figure 13(*d*). Since the envelope of the electric field oscillation decreases in amplitude monotonically in time, as shown in figure 11(*b*), the rate of energy transfer given by the form of C_E will also have an envelope that decreases in time. For a longer correlation interval τ, the average over a decreasing function will yield ever smaller values, leading to the decrease in the estimate of the total accumulated phase-space

https://doi.org/10.1017/S0022377816001197 Published online by Cambridge University Press

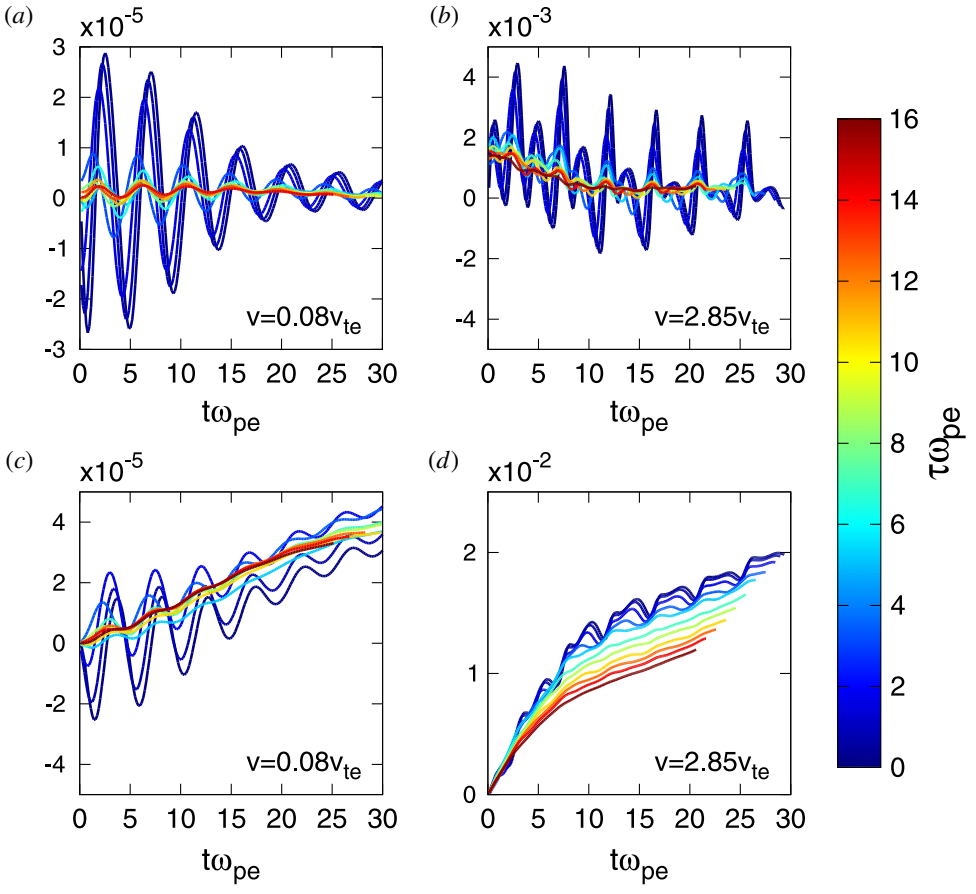

FIGURE 13. The correlation $C_E(v_0, t, \tau)$ from (3.20) over a range of correlation intervals $0 \leqslant \omega_{pe}\tau \leqslant 16$ at two velocity values, (*a*) off-resonance at $v_0 = 0.08v_{te}$ and (*b*) on-resonance at $v_0 = 2.85v_{te}$. Also, the change in the electron phase-space energy density $\Delta w_e(x_0, v, t)$ as a function of time $\omega_{pe}t$ at the same two velocity values, (*c*) off-resonance at $v_0 = 0.08v_{te}$ and (*d*) on-resonance at $v_0 = 2.85v_{te}$. Units of the energy transfer rate (*a*,*b*) and change in phase-space energy density (*c*,*d*) are arbitrary, but consistent from one panel to another.

energy density change seen in figure 13(*d*). Therefore, one should not choose a correlation interval that is much longer than the lifetime of a damped wave. In a turbulent plasma, however, the nonlinear interactions underlying the turbulent cascade of energy from large scales will continually feed energy into the fluctuations at the scales where collisionless damping can occur, so this constraint is likely to be far less important for diagnosing collisionless damping in a turbulent plasma.

Now that we have determined an appropriate value for the correlation interval, we apply the field–particle correlation $C_E(v, t, \tau)$, given by (3.20), to the observable data in figure 11 using a correlation interval $\omega_{pe}\tau = 6.28$. The resulting value of the correlation $C_E(v, t, \tau)$ as a function of velocity v/v_{te} and time $\omega_{pe}t$ for Case I is shown in figure 14(*a*). The selection of an appropriately long correlation interval has eliminated the large oscillations seen in figure 12 at $v/v_{te} < 2$, showing that the remaining rate of secular energy transfer has a significant amplitude that is much more localized around the resonant velocity of $v/v_{te} = 2.86$. Further, we can time integrate

https://doi.org/10.1017/S0022377816001197 Published online by Cambridge University Press

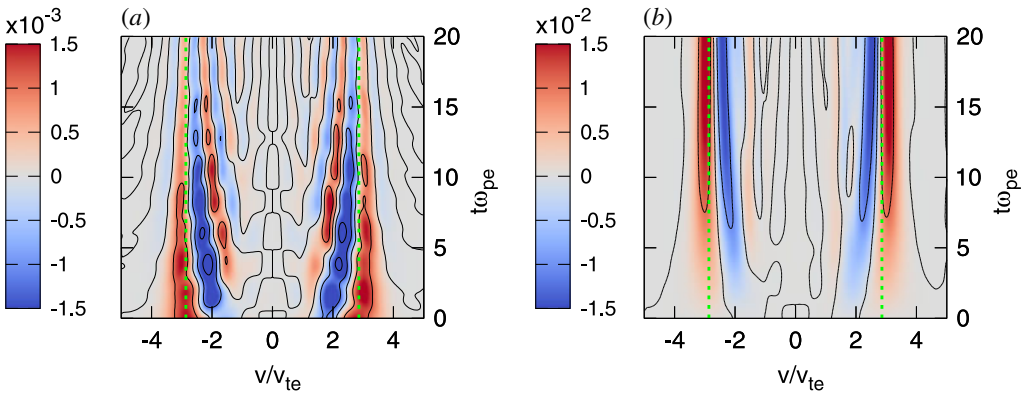

FIGURE 14. (*a*) The field–particle correlation $C_E(v,\, t,\, \tau) = C_\tau(q_s v^2/2\partial\delta f_s/\partial v,\, E)$ at $x = 0$ using a correlation interval $\omega_{pe}\tau = 6.28$. (*b*) The time-integrated correlation $\int_0^t C_E(v, t', \tau)\,\mathrm{d}t'$, showing a clear resonant signature of the secular energy transfer about the resonant velocities $v = \pm\omega/k$ (dashed green).

this correlation to obtain the secular change in the electron phase-space energy density, $\Delta w_e(x_0, v, t)$, shown in figure 14(*b*). Panel (*b*) is the primary result of this field–particle correlation technique, showing the net change in electron phase-space energy density is tightly correlated with the resonant velocity. The loss of energy at $v < \omega/k$ and gain of energy at $v > \omega/k$ corresponds physically to a flattening of the distribution function at the resonant velocity, consistent with the quasilinearly averaged electron distribution function shown in figure 3.

As mentioned in § 3.4, it may be impractical to compute the derivative of the perturbed distribution function, $\partial\delta f_s(x,\, v,\, t)/\partial v$, using spacecraft measurements that are affected by noise and typically have limited velocity-space resolution. Therefore, the alternative correlation $C'_E(v,\, t,\, \tau)$, given by (3.21), may be more suitable for the analysis of single-point spacecraft measurements. Therefore, we repeat the field–particle correlation analysis, starting with the observable single-point measurements given in figure 11, and using the alternative form of the correlation $C'_E(v,\, t,\, \tau)$ with the same correlation interval $\omega_{pe}\tau = 6.28$. In figure 15, we plot (*a*) the correlation $C'_E(v,\, t,\, \tau)$ as a function of velocity v/v_{te} and time $\omega_{pe}t$ and (*b*) the time-integrated correlation $\int_0^t C'_E(v,\, t',\, \tau)\,\mathrm{d}t'$ for Case I. This alternative form C'_E of the field–particle correlation analysis does not represent the rate of change of phase-space energy density, although its velocity-integrated value does yield the same net local energy transfer as correlation C_E. Nonetheless, this alternative form still yields a signature that is highly peaked at the resonant velocities $v = \pm\omega/k$, indicating that the physical mechanism of the secular energy transfer is a resonant process. In addition, of course, the velocity-integrated rate of energy change is the same for both forms of the correlation, so the total secular transfer of energy from collisionless interactions between the fields and particles can still be determined from the alternative form of the correlation $C'_E(v, t, \tau)$.

To show that this field–particle correlation method indeed recovers the local energy transfer rate, in figure 16(*a*) we plot the velocity-integrated correlation $\int \mathrm{d}v\, C_E(v, t, \tau)$ (red dotted), which provides a measure of the local (at position $x_0 = 0$) rate of transfer of spatial energy density from the electrostatic field to the electrons. We also plot the velocity-integrated value of the alternative correlation, $\int \mathrm{d}v\, C'_E(v, t, \tau)$ (blue dashed),

https://doi.org/10.1017/S0022377816001197 Published online by Cambridge University Press

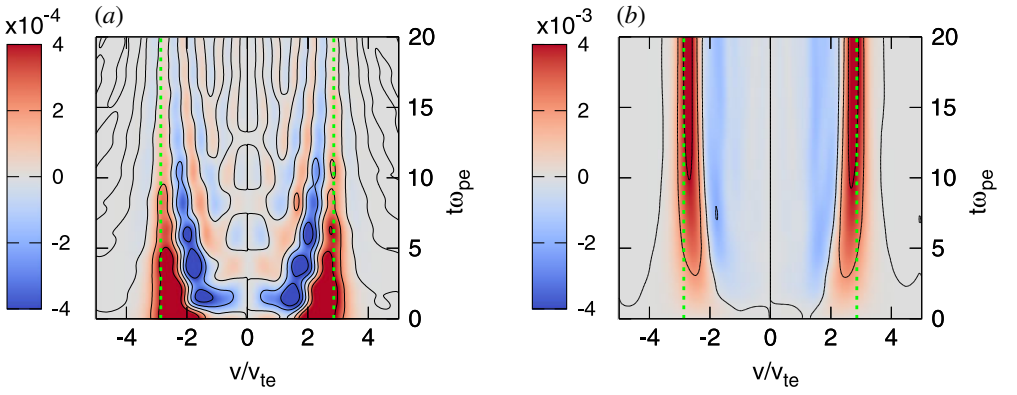

FIGURE 15. For Case I, (*a*) the alternative field–particle correlation $C'_E(v,\ t,\ \tau) = C_\tau(q_s v \delta f_s/\partial v, E)$ at $x = 0$ using a correlation interval $\omega_{pe}\tau = 6.28$. (*b*) The time-integrated correlation $\int_0^t C'_E(v,\ t',\ \tau)\,\mathrm{d}t'$. Vertical dashed green lines denote the resonant velocities $v = \pm\omega/k$.

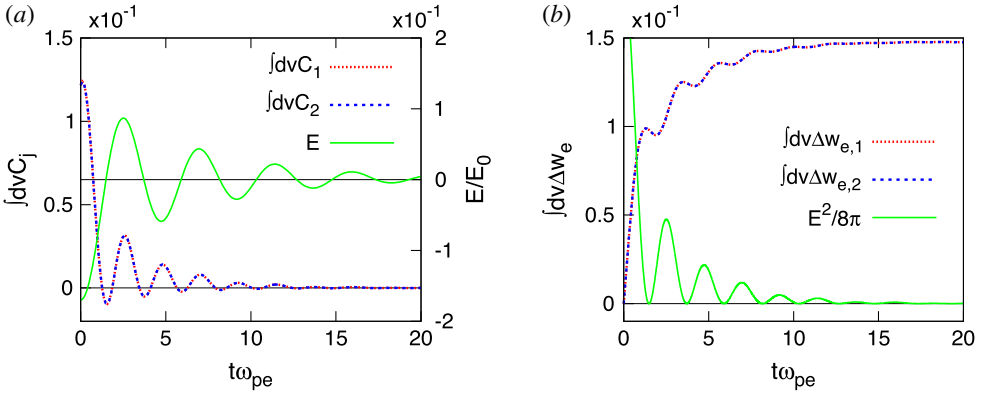

FIGURE 16. (*a*) The net local energy transfer rate, computed using the velocity-integrated correlation $\int \mathrm{d}v\, C_E(v, t, \tau)$ (red dashed) and alternative correlation, $\int \mathrm{d}v\, C'_E(v, t, \tau)$ (blue dashed). Also plotted on the right-hand vertical axis is the electric field amplitude as a function of time, E/E_0 (green). (*b*) The net accumulated transfer of spatial energy density, $\int \mathrm{d}v\, \Delta w_{ej}(x_0, v, t) = \int \mathrm{d}t' \int \mathrm{d}v\, C_j(c, t', \tau)$ for both C_E (red dotted) and C'_E (blue dashed) and local electrostatic spatial energy density, $|E(x_0, t)|^2/8\pi$ (green).

to demonstrate that these two alternative forms, when integrated over velocity, indeed yield the same result for the rate of transfer of spatial energy density between the fields and particles. Also plotted is the electric field amplitude as a function of time, E/E_0 (green), where the electric field is normalized to $E_0 = T_e/(q_e\lambda_{de})$. In figure 16(*b*), we plot the net accumulated transfer of spatial energy density, $\int \mathrm{d}v\, \Delta w_{ej}(x_0, v, t) = \int \mathrm{d}t' \int \mathrm{d}v\, C_j(c, t', \tau)$ for both C_E (red dotted) and C'_E (blue dashed). Also plotted is the local electrostatic spatial energy density, $|E(x_0, t)|^2/8\pi$ (green), showing that energy is lost from the electrostatic field while it is gained by the electrons. Note, however, that the accumulated local energy changes in the electrons and the electrostatic field do not sum to a constant value – this is because the ballistic and linear wave–particle

https://doi.org/10.1017/S0022377816001197 Published online by Cambridge University Press

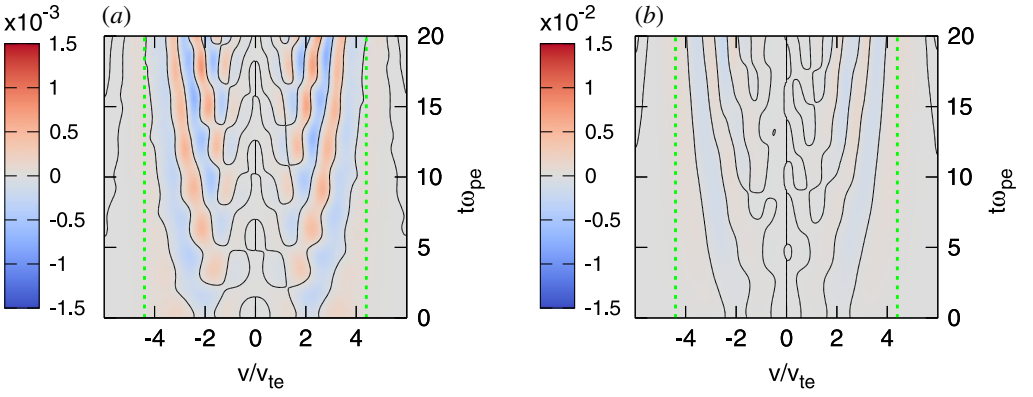

FIGURE 17. (*a*) The field–particle correlation $C_E(v,t,\tau) = C_\tau(q_s v^2/2\partial\delta f_s/\partial v, E)$ for Case II at $x = 0$ using a correlation interval $\omega_{pe}\tau = 6.28$. (*b*) The time-integrated correlation $\int_0^t C_E(v,t',\tau)\,\mathrm{d}t'$, showing a negligible signature of secular energy transfer at the resonant velocities $v = \pm\omega/k$ (dashed green).

interaction terms in (3.19) are non-zero locally. Only upon integrating over space is total energy conserved, as shown in figure 1.

6.2. *Case II: weakly damped standing Langmuir wave*

For the weakly damped standing Langmuir wave pattern described in § 5.2, we can perform the same field–particle correlation analysis. In figure 17, we plot (*a*) the field–particle correlation $C_E(v,t,\tau)$ using a correlation interval $\omega_{pe}\tau = 6.28$, and (*b*) the time-integrated correlation $\int_0^t C_E(v,t',\tau)\,\mathrm{d}t'$ for the weakly damped Case II. Note that the colour map magnitude of this figure is the same as that in figure 14, showing that the secular energy transfer for this weakly damped case is very small compared to the moderately damped Case I. The rate of energy transfer in panel (*a*) indeed shows some signal associated with the oscillating energy transfer that is not eliminated using a correlation interval of $\omega_{pe}\tau = 6.28$, but the time integration of the correlation in panel (*b*) effectively eliminates any net energy transfer accumulating over time. Note that this field–particle correlation technique produces only a very-small-amplitude signature in this weakly damped case, a signature that is unlikely to be observable given realistic instrumental limitations on the measurement of small-amplitude fluctuations in the velocity distribution function.

The field–particle correlation method indeed shows a negligible amount of local secular transfer of energy from fields to particles on the time scale of the wave period, as shown by plotting the velocity-integrated correlation $\int \mathrm{d}v\, C_E(v,t,\tau)$ (red dotted) in figure 18(*a*) and the net accumulated transfer of spatial energy density, $\int \mathrm{d}v\, \Delta w_e(x_0,v,t) = \int \mathrm{d}t' \int \mathrm{d}v\, C_E(c,t',\tau)$ in figure 18(*b*). Instrumental constraints likely would render any such small energy transfer rate unobservable.

6.3. *Case III: moderately damped single Langmuir wave mode*

Finally, we apply the field–particle correlation analysis to Case III, the propagating single Langmuir wave mode. The observable single-point measurements at $x = 0$ are plotted in figure 19, showing (*a*) the total perturbed electron distribution function

https://doi.org/10.1017/S0022377816001197 Published online by Cambridge University Press

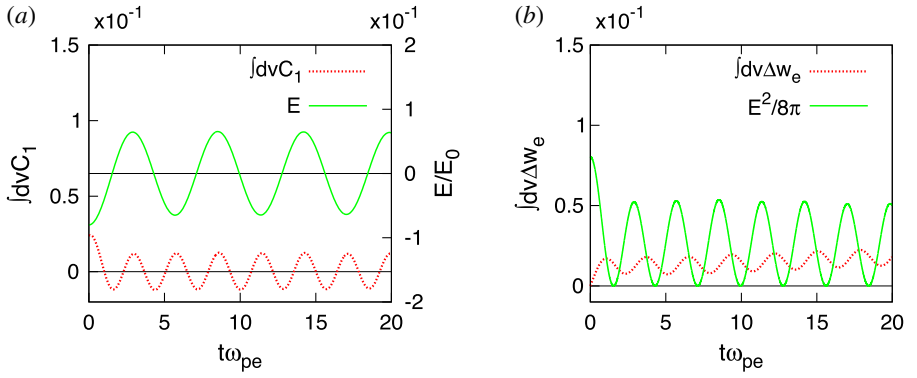

FIGURE 18. (*a*) The net local energy transfer rate, computed using the velocity-integrated correlation $\int \mathrm{d}v\, C_E(v, t, \tau)$ (red dashed) and the electric field amplitude as a function of time, E/E_0 (green). (*b*) The net accumulated transfer of spatial energy density, $\int \mathrm{d}v \Delta w_e(x_0, v, t) = \int \mathrm{d}t' \int \mathrm{d}v\, C_E(c, t', \tau)$ (red dotted) and local electrostatic spatial energy density, $|E(x_0, t)|^2/8\pi$ (green).

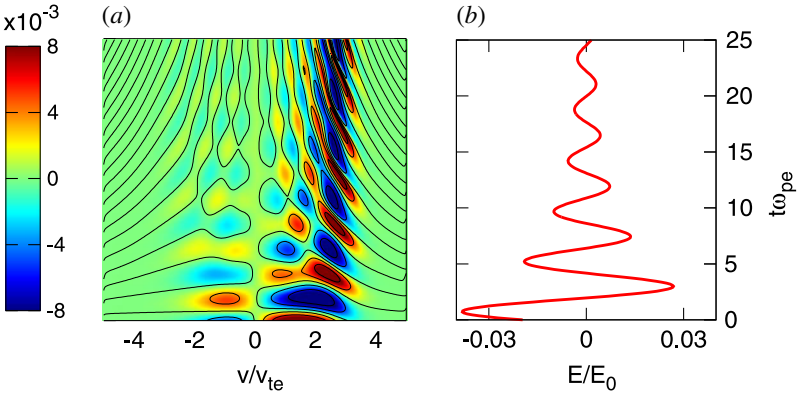

FIGURE 19. For Case III, (*a*) the total perturbed electron distribution function $\delta f_e(0, v, t)$ (colour map) and (*b*) electric field $E(0, t)$ measured at $x = 0$ as a function of normalized time $\omega_{pe}t$.

$\delta f_e(0, v, t)$ (colour map) and (*b*) the electric field $E(0, t)$ as a function of normalized time $\omega_{pe}t$. Note that the perturbed electron distribution function is highly localized in velocity near the resonant velocity, $v/v_{te} = \omega/(kv_{te}) = 2.86$.

For this case, we plot in figure 20 the products of the quantities used in the correlations $C_E(v, t, \tau)$ and $C'_E(v, t, \tau)$: (*a*) $(-q_s v^2/2)(\partial \delta f_s(0, v, t)/\partial v)E(0, t)$ and (*b*) $q_s v \delta f_s(0, v, t)E(0, t)$ as a function of velocity v/v_{te} and time $\omega_{pe}t$. In this case, even without the time average over the correlation interval, the product has a definite net sign on either side of the resonant velocity $v = \omega/k$ (dash-dotted green). Note that in this section we also plot the resonant velocity of the counterpropagating Langmuir wave, $v = -\omega/k$, because a very slight signature does appear in the opposite direction, likely due to an imperfect initialization of the single propagating Langmuir wave. Note that this minor amount of energy in the counterpropagating Langmuir wave does not impact the results of this study.

https://doi.org/10.1017/S0022377816001197 Published online by Cambridge University Press

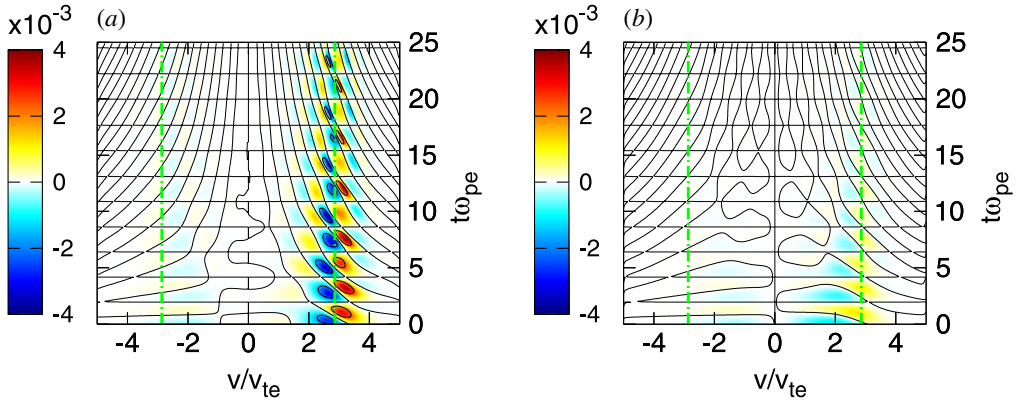

FIGURE 20. For Case III, plots of (*a*) the $C_E(v,\ t,\ \tau)$ correlation quantity, $(q_s v^2/2)(\partial \delta f_s(0,\ v,\ t)/\partial v)E(0,\ t)$ and (*b*) the $C'_E(v,\ t,\ \tau)$ correlation quantity, $q_s v \delta f_s(0,\ v,\ t)E(0,\ t)$, at $x = 0$ as a function of velocity v/v_{te} and time $\omega_{pe}t$. The dot-dashed vertical green line at $v = \omega/k$ denotes the resonant velocity of the initialized Langmuir wave mode, and we also plot $v = -\omega/k$ since nonlinear couplings may excite the counterpropagating Langmuir wave mode.

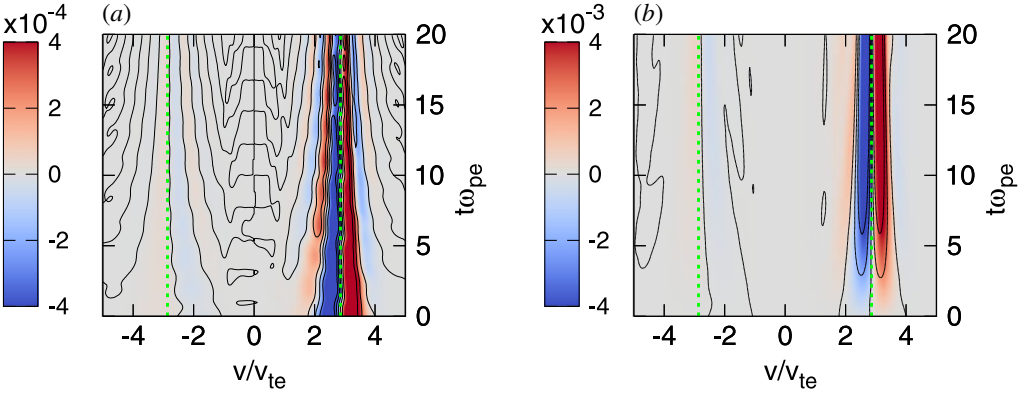

FIGURE 21. For Case III, (*a*) the field–particle correlation $C_E(v,\ t,\ \tau) = C_\tau(q_s v^2/2 \partial \delta f_s/\partial v,\ E)$ at $x = 0$ using a correlation interval $\omega_{pe}\tau = 6.28$. (*b*) The time-integrated correlation $\int_0^t C_E(v,\ t',\ \tau)\,\mathrm{d}t'$, showing a clear resonant signature of the secular energy transfer about the resonant velocity $v = \omega/k$ (dashed green).

In figure 21, we present the results of the field–particle correlation $C_E(v, t, \tau)$, given by (3.20), applied to Case III, the propagating single Langmuir wave mode using a correlation interval $\omega_{pe}\tau = 6.28$. We plot (*a*) the field–particle correlation $C_E(v, t, \tau)$, and (*b*) the time-integrated correlation $\int_0^t C_E(v, t', \tau)\,\mathrm{d}t'$ for Case III. In both (*a*) the rate of secular energy transfer and (*b*) the time-integrated net change in phase-space energy density, the resonant signature of Landau damping of the Langmuir wave is very clear, with the loss of energy at $v < \omega/k$ and the gain of energy at $v > \omega/k$ corresponding to a flattening of the distribution function at the resonant velocity. Finally, we plot in figure 22 the results of the alternative form of the correlation $C'_E(v, t, \tau)$, with (*a*) the correlation $C'_E(v, t, \tau)$ as a function of velocity v/v_{te} and

https://doi.org/10.1017/S0022377816001197 Published online by Cambridge University Press

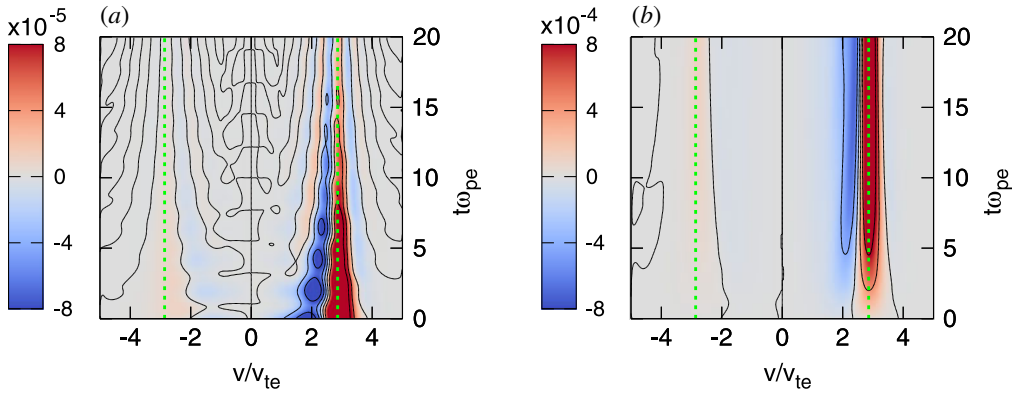

FIGURE 22. For Case III, (*a*) the alternative field–particle correlation $C_E'(v,\, t,\, \tau) = C_\tau(q_s v \delta f_s/\partial v, E)$ at $x = 0$ using a correlation interval $\omega_{pe}\tau = 6.28$. (*b*) The time-integrated correlation $\int_0^t C_E'(v,\, t',\, \tau)\, \mathrm{d}t'$. Vertical dashed green line denotes the resonant velocity $v = \omega/k$.

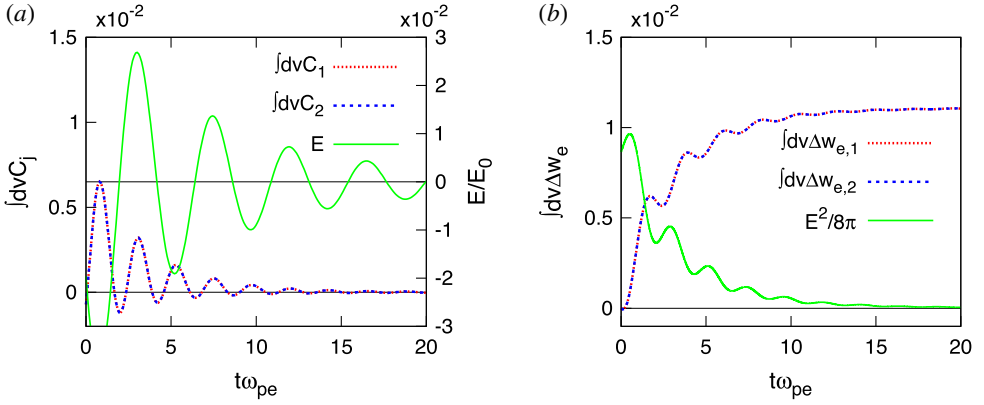

FIGURE 23. (*a*) The net local energy transfer rate, computed using the velocity-integrated correlation $\int \mathrm{d}v\, C_E(v,\, t,\, \tau)$ (red dashed) and alternative correlation, $\int \mathrm{d}v\, C_E'(v,\, t,\, \tau)$ (blue dashed). Also plotted is the electric field amplitude as a function of time, E/E_0 (green). (*b*) The net accumulated transfer of spatial energy density, $\int \mathrm{d}v\, \Delta w_{ej}(x_0,\, v,\, t) = \int \mathrm{d}t' \int \mathrm{d}v\, C_j(c, t', \tau)$ for both C_E (red dotted) and C_E' (blue dashed), and local electrostatic spatial energy density, $|E(x_0, t)|^2/8\pi$ (green).

time $\omega_{pe}t$ and (*b*) time-integrated correlation $\int_0^t C_E'(v, t', \tau)\, \mathrm{d}t'$ for Case III. Again, we see that this alternative form has a peak in the energy transfer rate and net transferred energy at the resonant velocity $v = \omega/k$ (dotted green), indicating clearly the resonant nature of the mechanism of collisionless energy transfer.

In figure 23, we show the local (at position $x_0 = 0$) rate of transfer of spatial energy density from the electrostatic field to the electrons by plotting (*a*) the velocity-integrated correlation $\int \mathrm{d}v\, C_E(v,\, t,\, \tau)$ (red dotted) and the alternative correlation, $\int \mathrm{d}v\, C_E'(v, t, \tau)$ (blue dashed). Also plotted is the electric field amplitude as a function of time, E/E_0 (green). In figure 23(*b*), we plot the net accumulated transfer of spatial energy density, $\int \mathrm{d}v\, \Delta w_{ej}(x_0,\, v,\, t) = \int \mathrm{d}t' \int \mathrm{d}v\, C_j(c,\, t',\, \tau)$ for

https://doi.org/10.1017/S0022377816001197 Published online by Cambridge University Press

both C_E (red dotted) and C'_E (blue dashed). Also plotted is the local electrostatic spatial energy density, $|E(x_0, t)|^2/8\pi$ (green), showing that energy is lost from the electrostatic field while it is gained by the electrons.

7. Discussion

This paper proposes a novel field–particle correlation technique that uses single-point measurements of the particle velocity distribution functions and electromagnetic fields to isolate the secular energization of the plasma particles due to the damping of the electromagnetic fields and to provide vital new information about how this energy transfer is distributed as a function of particle velocity. The technique has been developed using guidance from kinetic plasma theory to estimate the rate of energy transfer between electromagnetic fields and plasma particles, using a correlation over time to average out the oscillating energy transfer that supports wave motion, isolating the secular transfer of energy associated with the collisionless damping of electromagnetic fluctuations and resulting energization of particles. This extremely general technique has been worked out theoretically in detail for the case of electrostatic fluctuations in an unmagnetized, 1D-1V Vlasov–Poisson plasma in § 3. The application of the resulting field–particle correlation procedure to single-point measurements generated using nonlinear simulations of Langmuir wave damping in a 1D-1V Vlasov–Poisson plasma is presented in § 6, demonstrating that this method can determine the local energization of the plasma particles as a function of particle velocity, providing valuable insight into the nature of the collisionless damping mechanism. Here we discuss the extension of this general field–particle correlation technique to the case of the collisionless damping of turbulent fluctuations in the magnetized plasma of the solar wind.

In the weakly collisional, magnetized plasma of the solar wind, three distinct physical mechanisms have been proposed to be responsible for the dissipation of plasma turbulence: (i) resonant collisionless wave–particle interactions, such as Landau damping, transit-time damping or cyclotron damping (Landau 1946; Barnes 1966; Coleman Jr. 1968; Denskat, Beinroth & Neubauer 1983; Isenberg & Hollweg 1983; Goldstein, Roberts & Fitch 1994; Leamon *et al.* 1998*b*,*a*; Quataert 1998; Gary 1999; Leamon *et al.* 1999; Quataert & Gruzinov 1999; Leamon *et al.* 2000; Isenberg, Lee & Hollweg 2001; Hollweg & Isenberg 2002; Howes *et al.* 2008*a*; Schekochihin *et al.* 2009; TenBarge & Howes 2013; Howes 2015; Li *et al.* 2016); (ii) non-resonant collisionless wave–particle interactions, primarily leading to stochastic ion heating (Chen, Lin & White 2001; Johnson & Cheng 2001; White, Chen & Lin 2002; Voitenko & Goossens 2004; Bourouaine, Marsch & Vocks 2008; Chandran 2010; Chandran *et al.* 2010, 2011; Bourouaine & Chandran 2013); and (iii) dissipation in coherent structures, specifically current sheets, often involving collisionless magnetic reconnection (Dmitruk, Matthaeus & Seenu 2004; Markovskii & Vasquez 2011; Matthaeus & Velli 2011; Osman *et al.* 2011; Servidio *et al.* 2011; Osman *et al.* 2012*a*,*b*; Wan *et al.* 2012; Karimabadi *et al.* 2013; Zhdankin *et al.* 2013; Osman *et al.* 2014*a*,*b*; Zhdankin, Uzdensky & Boldyrev 2015*a*; Zhdankin *et al.* 2015*b*).

As discussed in § 2, under the weakly collisional conditions of the solar wind, all of these mechanisms are mediated by the Lorentz force term in the Boltzmann equation (2.1). Therefore, all of these collisionless damping mechanisms will necessarily lead to a correlation between fluctuations in the particle velocity distribution functions and the electromagnetic fields. Each different physical mechanism, however, is likely to generate a distinct velocity-space signature that can be diagnosed

https://doi.org/10.1017/S0022377816001197 Published online by Cambridge University Press

using the general approach of field–particle correlations. For example, Landau damping is expected to generate fluctuations in the distribution function that vary along the direction parallel to the local magnetic field, whereas cyclotron damping leads to pitch angle scattering that can also generate variations in the distribution function in the perpendicular direction. These distinct velocity-space signatures of the field–particle correlation can be used to identify the dominant physical mechanism responsible for the damping of the turbulent fluctuations.

The concept of using field–particle correlations to diagnose the secular transfer of energy between fields and particles is very general. The field–particle correlation technique described in this paper was derived directly from (3.19), a nonlinear phase-space energy density transport equation derived from the Boltzmann equation, and assumed nothing about the existence of waves or the specific properties of Landau damping. Nonetheless, the particular form of the field–particle correlation can be optimized to isolate each of the different mechanisms depending on the specific properties of each mechanism. For example, Landau damping is a resonant interaction involving the force on a charged particle by the component of the electric field parallel to the magnetic field, $E_\parallel$. On the other hand, transit-time damping is due to the magnetic mirror force acting on the magnetic moment of the particle's gyration about magnetic field, involving parallel gradients of the magnetic field magnitude, dominated by $\delta B_\parallel$ in the limit of $|\delta \boldsymbol{B}| \ll |\boldsymbol{B}|$. The particular field–particle correlation demonstrated here is the ideal diagnostic for Landau damping of electrostatic fluctuations in a Vlasov–Poisson plasma. For the case of the collisionless damping of fluctuations in the weakly collisional solar wind, insights from kinetic theory will be necessary to devise the most discerning forms of field–particle correlations for each of the three major proposed damping mechanisms above, as well as stochastic ion heating and collisionless magnetic reconnection.

Below we will comment on the generalizations necessary to apply the field–particle correlation technique to diagnose the collisionless damping of turbulent fluctuations in the solar wind using single-point measurements of particle velocity distribution functions and electromagnetic fields. We also will enumerate a number of caveats regarding the use of this novel field–particle correlation method in the solar wind. Finally, we will mention a couple of potential analysis techniques that can be used in concert with field–particle correlations.

7.1. *Measurements in a moving frame and the Taylor hypothesis*

A key issue regarding the applicability of this field–particle correlation method to diagnose the collisionless energy transfer in the solar wind is the fact that measurements are made in the frame of reference of the spacecraft, but the solar wind is flowing radially outward from the sun at a speed ranging approximately from 300 to 800 km s^{-1}, where the typical Alfvén speed in the wind is around 50 km s^{-1}. In studies of solar wind turbulence, this super-Alfvénic flow is often exploited to interpret the temporal fluctuations measured by the spacecraft as the result of spatial fluctuations being swept past the spacecraft by the solar wind flow, an approximation known as the Taylor hypothesis (Taylor 1938). An important question is whether this field–particle correlation technique still works when the single point of measurement is moving with respect to the plasma frame.

In fact, if applied carefully, we expect this field–particle correlation technique to be actually rather insensitive to measurements made in a frame of reference moving relative to the plasma frame. There are three separate points related to this issue

https://doi.org/10.1017/S0022377816001197 Published online by Cambridge University Press

of the Taylor hypothesis. First, how does the movement of the measurement point affect the process of averaging out the oscillating energy transfer over the correlation interval? Second, can the technique be applied to analyse spatially intermittent heating, such as the localization of heating near current sheets found in numerical simulations of plasma turbulence (Uritsky *et al.* 2010; Wan *et al.* 2012; Karimabadi *et al.* 2013; TenBarge & Howes 2013; Wu *et al.* 2013; Zhdankin *et al.* 2013) and inferred from solar wind measurements (Borovsky & Denton 2011; Osman *et al.* 2011; Perri *et al.* 2012; Wang *et al.* 2013; Wu *et al.* 2013)? Third, the frame of reference of the particle velocity and electromagnetic field measurements used in the correlation must be consistent.

To isolate the secular energy transfer arising from the collisionless damping of electromagnetic fluctuations, the key step in the technique is to perform the correlation over a suitably long correlation interval τ in order to average out the generally larger-amplitude oscillating energy transfer. In the examples presented here, this step is achieved by averaging in time over a correlation interval longer than the period of the wave, $\tau > T$. But, fundamentally, the only requirement is that the measurements span more than 2π of the wave phase. For the Langmuir waves of the 1D-1V Vlasov–Poisson system presented in § 6, the wave phase is a function of both the time and position, $\alpha(x, t) = kx - \omega t$. Thus, any combination of changes in time and position that cover more than 2π of the wave phase will suffice to average out the oscillating energy transfer. A perfectly suitable alternative is to use measurements at a series of positions x_j (all measured at the same time t_0), thereby using a spatial average, instead of a time average, to eliminate the oscillating energy transfer; this is, in fact, exactly the averaging process that is performed in quasilinear theory. But such spatially distributed measurements are not accessible for most spacecraft missions – this motivates the time-averaged form of the procedure presented here. But, if the point of measurement is moving in space, $x_0(t)$, then the phase of the wave, for a time series of measurements, is given by $\alpha(t) = kx_0(t) - \omega t$, and the field–particle correlation technique presented here simply requires this phase α to span more than 2π over the correlation interval τ.

Another important question is whether this field–particle correlation method can be used to diagnose the particle energization in localized structures, such as current sheets. If the current sheet is particularly thin, obviously the cadence of the particle measurements has to be sufficiently high to sample within the structure of interest as it is advected past the spacecraft with the solar wind flow. Fortunately, current and upcoming spacecraft missions – such as MMS, Solar Probe Plus, Solar Orbiter and THOR – have sufficiently high-cadence plasma instruments to satisfy this unavoidable requirement. The crucial issue for applying field–particle correlations in the case of spatially intermittent particle energization is to determine an appropriate correlation interval τ to isolate the secular transfer of energy from the oscillating transfer of energy. For wave-like turbulent fluctuations in which there is a conservative transfer of energy from fields to particles and back, the correlation interval τ must be sufficiently long to expose the often smaller-amplitude secular energy transfer associated with the collisionless damping of the turbulence. But the energy transfer in a current sheet has a significantly different character: the particle energization at current sheets often appears to be sign-definite, and may have an amplitude that is large relative to any oscillating energy transfer associated with superimposed wave-like fluctuations. These characteristics are supported by Cluster observations of particle energization at a reconnecting current sheet in magnetosheath turbulence (Retinò *et al.* 2007; Sundkvist *et al.* 2007) as well as simulations of a current sheet generated by the

https://doi.org/10.1017/S0022377816001197 Published online by Cambridge University Press

strong nonlinear interaction between counterpropagating Alfvén waves (Howes 2016). In both cases, the local energy transfer rate, given by evaluating $\boldsymbol{j} \cdot \boldsymbol{E}$ within the current sheet, is largely sign-definite, implying the transfer of energy from the electromagnetic fields to the particles. In this case, the correlation interval need not be large, and in fact, significant secular particle energization may be apparent without any averaging of the measured single-point time series. Therefore, with appropriate modifications respecting the distinct nature of particle energization at current sheets, the field–particle correlation technique may indeed provide a valuable new tool for the exploration of particle energization at current sheets.

The last complication arising from using measurements made in the spacecraft frame of reference, in relative motion with respect to the solar wind plasma frame, is that it is imperative to use a consistent frame of reference for both field and particle measurements. For example, often solar wind particle velocity distribution functions are transformed to the frame of reference of the bulk solar wind plasma flow[†], $\boldsymbol{v}_{sw}$. But electric field measurements are made in the spacecraft frame moving at a speed of hundreds of km s^{-1} relative to the solar wind plasma. Thus, any electric field measurements to be used must be Lorentz transformed from the spacecraft to the plasma frame, $\boldsymbol{E}' \simeq \boldsymbol{E} + \boldsymbol{v}_{sw}/c \times \boldsymbol{B}$ (Chen *et al.* 2011; Howes, Klein & TenBarge 2014). The plasma-frame electric field $\boldsymbol{E}'$ is often much smaller than both the electric field measured in the spacecraft frame $\boldsymbol{E}$ and the convection electric field $\boldsymbol{v}_{sw}/c \times \boldsymbol{B}$, so uncertainties in the determination of the solar wind velocity $\boldsymbol{v}_{sw}$ can make the determination of the plasma-frame electric field $\boldsymbol{E}'$ unreliable. To avoid this complication, one may use a component of the magnetic field – under typical solar wind parameters, a Lorentz transform changes the magnetic field negligibly (Howes *et al.* 2014) – as a proxy for the desired electric field component, at the expense of making an assumption that the electromagnetic wave satisfies a linear wave eigenfunction.

7.2. *Generalization to solar wind measurements*

First, spacecraft measurements can provide three-dimensional velocity (3V) distribution functions $f_s(v_x, v_y, v_z)$, so one must appropriately adapt the field–particle correlations given in (3.20) and (3.21). The Lorentz force term in the Boltzmann equation (2.1) respects the direction of the local magnetic field, so transformation of the distribution function to field-aligned coordinates, $f_s(v_{\perp 1}, v_{\perp 2}, v_\parallel)$, is generally helpful in the interpretation of the measurements. Following this step, one means of adapting the correlation is simply to determine the field–particle correlation at each point in the 3V space, $C_E(v_{\perp 1}, v_{\perp 2}, v_\parallel, t, \tau)$. Then, one may choose to reduce this 3V correlation, for example determining a parallel correlation $C_E(v_\parallel, t, \tau)$ by integrating over the perpendicular dimensions of velocity space. Alternatively, this reduction can be performed first to obtain the parallel reduced distribution function $f_s(v_\parallel)$ – yielding a valuable improvement in the signal-to-noise ratio of the particle velocity measurements – followed by a correlation of an appropriate electromagnetic field component with the reduced velocity distribution. Tests of these alternatives using existing spacecraft datasets may enable the best approach to be identified.

Second, with spacecraft instrumentation it is often not possible to reliably detect $E_\parallel$ directly because it generally has a much smaller magnitude than its components perpendicular to the local magnetic field. In this case, it is possible to use another

[†]Note that this bulk solar wind plasma flow value may also include transverse motions (relative to the magnetic field direction) associated with turbulent Alfvénic fluctuations.

https://doi.org/10.1017/S0022377816001197 Published online by Cambridge University Press

component of the electromagnetic fields, such as $E_\perp$ or $\delta B_\parallel$, as a proxy for $E_\parallel$ (or whatever other component you desire that is difficult to measure directly). Maxwell's equations dictate the relationships between the different components of the electric and magnetic fields; the spatial gradients necessary to specify these relationships completely, however, are not observationally available when restricted to single-point spacecraft measurements. Nonetheless, the linear response of the plasma and electromagnetic fields to an applied perturbation can be computed theoretically given the frequency and wavevector of the perturbation. If one assumes a particular linear wave mode and wavevector, one can predict the relationship between all of the different components of the electric and magnetic fields. One can thereby relate the phase and amplitude of the desired field in terms of a more easily measured field, for example $E_\parallel$ in terms of $E_\perp$. Additionally, this assumption can be tested by comparing the phase and amplitude relationships of all of the other measured field components. The strategy of assuming that the relationships among field components satisfy the eigenfunctions of linear wave modes has meet with significant success in establishing the kinetic-Alfvén-wave nature of dissipation range fluctuations in the solar wind (Salem *et al.* 2012; Chen *et al.* 2013) and the slow-mode nature of compressible fluctuations in the solar wind inertial range (Howes *et al.* 2012; Klein *et al.* 2012). Additionally, nonlinear gyrokinetic simulations of solar wind turbulence have demonstrated that the different field components indeed have amplitude relationships as a function of scale that are given by the linear Alfvén and kinetic Alfvén wave eigenfunctions (Howes *et al.* 2008*b*, 2011; TenBarge *et al.* 2012). Therefore, the specific form of the field–particle correlation can be modified to allow use with an alternative field component as a proxy for any component that cannot be easily measured.

7.3. *Caveats on the use of the field–particle correlation technique*

One significant benefit of the field–particle correlation method devised here is that, even if the cadence of plasma distribution function measurements Δt is longer than the period T of typical fluctuations on the scale at which the collisionless damping occurs, using a sufficiently long correlation interval $\tau \gg T$ may enable the signature of the secular energy transfer to be obtained. A first caveat, however, is that aliasing may become significant for under-sampled plasma measurements, artificially altering the phase of the fluctuations in the distribution function and thereby masking the underlying physical correlation (Klein *et al.* 2014).

A second caveat involves the application of the method to diagnose spatially localized dissipation. Even though the method uses single-point measurements to determine the local rate of energy transfer between fields and particles, the correlation must be performed over a time longer than the characteristic fluctuation frequency to isolate the typically small secular energy transfer from the often much larger oscillating energy transfer. The result may be that the correlation smears out the signature of strongly localized energy transfer in the attempt to average out the oscillating component. On the other hand, if the localized energy transfer is sign-definite and has a sufficiently large amplitude, it may still be discernible by comparing correlations computed over a range of time intervals.

Particle velocity distribution measurements that are highly resolved in pitch angle and energy often suffer from rather a low count rate, and consequently a low signal-to-noise ratio, in the low-density conditions of the solar wind plasma. A third caveat is that noise is particularly detrimental to extracting meaningful correlations

https://doi.org/10.1017/S0022377816001197 Published online by Cambridge University Press

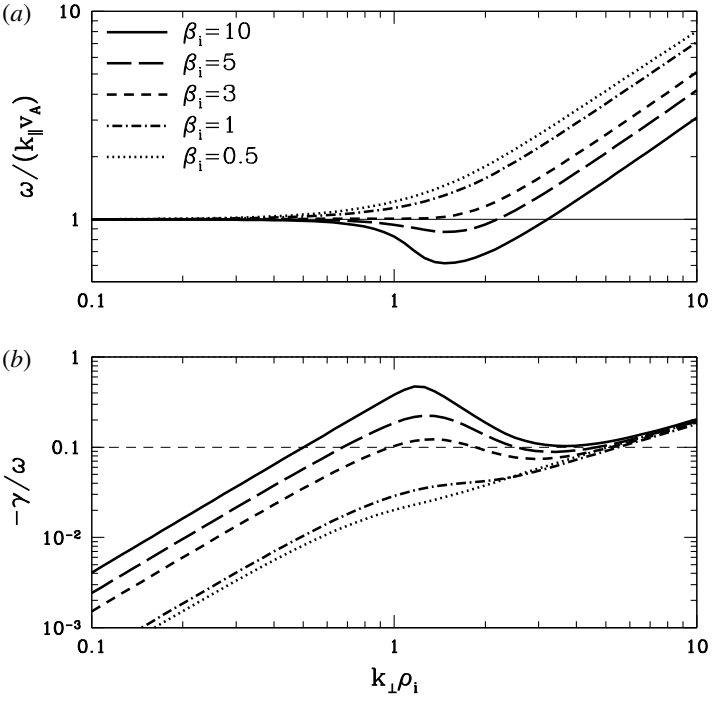

FIGURE 24. (*a*) Normalized phase velocity $\omega/k_\parallel v_A$ and (*b*) normalized damping rate $-\gamma/\omega$ versus perpendicular wavenumber $k_\perp\rho_i$ for the collisionless damping of the Alfvén and kinetic Alfvén wave for $\beta_i = 0.5, 1, 3, 5, 10$.

from measurements (Howes *et al.* 2012), so particular care must be taken to ensure that the measurement noise is low enough not to avoid corrupting the correlations.

A fourth significant caveat is that the broadband nature of the spectrum of turbulent fluctuations may smear out any resonant signatures of the dissipation. In particular, since the collisionless damping becomes significant in the same range of length scales that the characteristic linear response becomes dispersive, the change in wave phase velocity leads to a range of possible resonant velocities. However, significant transit-time damping of Alfvén waves onto ions occurs over a rather narrow band in perpendicular wavenumber, alleviating this potential problem. As an example, we calculate the linear frequencies and damping rates of Alfvén waves using the linearized Vlasov–Maxwell dispersion relation (Quataert & Gruzinov 1999; Howes *et al.* 2006) for $T_i/T_e = 1$ and $\beta_i = 0.5, 1, 3, 5, 10$ and a realistic mass ratio $m_i/m_e = 1836$. In figure 24, we plot the (*a*) normalized phase velocity $\omega/k_\parallel v_A$ and (*b*) normalized damping rate $-\gamma/\omega$ versus perpendicular wavenumber $k_\perp\rho_i$. The peak in the damping rate at $k_\perp\rho_i \sim 1$ for higher values of ion plasma beta $\beta_i \gtrsim 3$ is due to transit-time damping onto the ions. Significant collisionless transit-time damping occurs for $-\gamma/\omega > 0.1$ (thin dashed); the phase velocities corresponding to the strongly damped range of $k_\perp\rho_i$ vary by less than a factor of two, so indeed the range of phase velocities is rather narrow. Therefore, in this case, we expect that any signature of resonant energy transfer is unlikely to be obscured by dispersion in the phase velocity.

At higher values of $k_\perp\rho_i \gtrsim 5$ in figure 24, however, the damping strengthens again, yielding $-\gamma/\omega > 0.1$ due to Landau damping onto the electrons. In this case, the

https://doi.org/10.1017/S0022377816001197 Published online by Cambridge University Press

damping is not narrowband, but instead rises monotonically with increasing $k_\perp \rho_i$. The corresponding phase velocities of kinetic Alfvén waves at these scales also increase linearly with the perpendicular wavenumber, so the velocity-space signature of energy transfer by electron Landau damping using field–particle correlations may indeed be smeared out by this continual dispersive change of the resonant velocity.

A fifth and final caveat also deals with applying this field–particle correlation technique to single-point spacecraft measurements of the electron velocity distributions. Because the electron thermal velocity is much faster than the Alfvén velocity under typical solar wind plasma conditions, the resonant velocity for electron Landau damping of turbulent fluctuations falls within the core of the electron velocity distribution, $|\omega/k_\parallel| < v_{te}$. Spacecraft charging effects typically corrupt electron particle velocity measurements in the core of the distribution at $|v| < v_{te}$, so it is uncertain if a meaningful field–particle correlation can be computed in the presence of interference by spacecraft charging.

7.4. *Complementary analysis techniques*

Finally, we propose here two techniques that can be used to complement a field–particle correlation analysis of single-point spacecraft measurements in the turbulent solar wind. We have shown that the field–particle correlation $C_E(v, t, \tau)$ is a direct measure of the collisionless transfer of phase-space energy density between fields and particles in § 3.4, but it may not be possible to compute accurately the derivative $\partial \delta f_s(x, v, t)/\partial v$ necessary for this particular correlation. The alternative field–particle correlation $C'_E(v, t, \tau)$ is more easily applied to spacecraft measurements, but does not yield a direct measure of the energy transfer in velocity space. One may test whether the derivative $\partial \delta f_s(x, v, t)/\partial v$ in $C_E(v, t, \tau)$ is leading to inaccurate results by computing both forms of the correlation and integrating over velocity. Since they should both have the same velocity-integrated value of the local energy transfer rate, any disagreement is likely due to problems with the derivative.

A second method to determine whether the estimate of the rate of transfer of the phase-space energy density given by the field–particle correlation analysis is meaningful is to compare the correlation signature using a the same field measurements with randomized phases. To randomize the phases, the time series of field measurements can be Fourier transformed to a frequency spectrum, each complex Fourier coefficient can be multiplied by a random complex phase, and then the randomized Fourier frequency coefficients (which have the same energy spectrum as the original field measurements) can be inverse transformed back to the time domain. The envelope of the field–particle correlations computed using an ensemble of randomized fields gives an idea of the noise level in the correlation as a function of velocity.

8. Conclusion

In the quest to unravel the kinetic physics of the damping of turbulent fluctuations in weakly collisional space and astrophysical plasmas, we propose here an innovative field–particle correlation technique to estimate the resulting particle energization and identify the characteristics of the governing collisionless energy transfer mechanism. The major features of this novel method are:

(*a*) The method requires only single-point measurements of the fluctuations in the electromagnetic fields and particle velocity distribution functions, enabling it to be applied not only to numerical simulations but also to spacecraft measurements.

https://doi.org/10.1017/S0022377816001197 Published online by Cambridge University Press

(*b*) By correlating the field and particle fluctuations over a suitable time interval, the method averages out the conservative, oscillating energy transfer rate associated with wave motion to isolate the secular energy transfer rate associated with the collisionless damping of the electromagnetic fluctuations.

(*c*) By not requiring an integration over particle velocity, the procedure provides information about the energy transfer between electromagnetic fields and plasma particles as a function of particle velocity, yielding vital new information that can help to identify the dominant collisionless mechanism governing the damping of the turbulent fluctuations.

Using the simplified case of the electrostatic fluctuations in a 1D-1V Vlasov–Poisson plasma, we have shown how to use nonlinear kinetic plasma theory to derive a particular field–particle correlation that corresponds directly to the rate of transfer of energy density in phase space, given by $C_E(v_0, t, \tau)$ in (3.20). We have applied this field–particle correlation technique to a nonlinear simulation of the collisionless damping of Langmuir waves in a Vlasov–Poisson plasma, generating the key field–particle correlation results in figure 14.

We have outlined caveats on the applying this field–particle correlation technique to diagnose the secular transfer of energy from fields to particles associated with the collisionless damping of turbulent electromagnetic fluctuations in the solar wind. The concept of using field–particle correlations to diagnose the secular transfer of energy between fields and particles is very general, and is applicable to any proposed collisionless damping mechanism in the solar wind, including Landau damping, transit-time damping, cyclotron damping, stochastic ion heating and collisionless magnetic reconnection. Kinetic theory can be used to devise a suitable field–particle correlation for the investigation of a particular proposed mechanism. Specifically, one is free to specify whether to use 3-D velocity distributions $f(v_{\perp 1}, v_{\perp 2}, v_\parallel)$ or reduced parallel $f(v_\parallel)$ or perpendicular $f(v_\perp)$ velocity distributions, as well as the appropriate component of the electromagnetic field, or a more easily measurable proxy field component. Supporting numerical work will be required to characterize the qualitative and quantitative features of the field–particle correlations associated with each of the proposed damping mechanisms above.

We emphasize that this general technique can be applied to any weakly collisional plasma system in which the particle velocity distributions and electromagnetic fields can be measured at a single point in space. It can be widely used to estimate the local rate of transfer of energy density in phase space in kinetic numerical simulations not only of kinetic plasma turbulence (Howes 2015), but also of collisionless magnetic reconnection and particle acceleration. And it can also be used to investigate the weakly collisional dynamics in spacecraft measurements and laboratory experiments (Schroeder *et al.* 2016). A major motivation for the work presented here is to develop a mature field–particle correlation method that can be used as the primary tool for the analysis of measurements from current, upcoming and proposed spacecraft missions that are focused on the kinetic microphysics of weakly collisional heliospheric plasmas, including the Magnetospheric Multiscale (MMS), Solar Probe Plus, Solar Orbiter and Turbulent Heating ObserveR (THOR) missions.

Acknowledgements

We are grateful to J. W. R. Schroeder, F. Skiff, C. A. Kletzing, J. M. TenBarge, and D. Burgess for important discussions and comments on this topic. The work has been supported by NSF CAREER Award AGS-1054061, NSF AGS-1331355, and DOE DE-SC0014599.

Appendix A. Numerical implementation of the VP code

The numerical implementation of the nonlinear Vlasov–Poisson simulation code VP evolves the components of the total velocity distribution function for species s,

$$f_s(x, v, t) = f_{s0}(v) + \delta f_{sB}(x, v, t) + \delta f_{sWl}(x, v, t) + \delta f_{sWn}(x, v, t), \tag{A 1}$$

according to the separated evolution equations (4.2)–(4.4). Note that the VP code can also be run in a linear mode simply by setting $\delta f_{sWn}(x, v, t) = 0$. The 1D-1V domain is discretized with uniform spacing over the interval $[-L/2, L/2]$ in physical space x using n_x points and over $[-v_{max}, v_{max}]$ in velocity space v using $n_v + 1$ points. Spatial derivatives are computed using second-order centred finite differencing, periodically wrapped at the spatial boundary. Velocity derivatives are computed using second-order centred finite differencing, except for the points at $v = \pm v_{max}$, which employ only first-order finite differencing. The distribution function is advanced using a third-order Adams–Bashforth scheme. The maximum time step for this explicit algorithm is constrained by the Courant–Friedrichs–Lewy stability criterion to be $(\Delta t)_{max} = \Delta x / \max(v_{max}, \omega/k)$, where the maximum velocity is either the maximum resolved particle velocity v_{max} or the maximum phase velocity of the Langmuir wave mode, ω/k. The time step used in the simulation is set to be some fraction f_{CFL} of this maximum time step, $\Delta t = f_{CFL}(\Delta t)_{max}$. At each time step, the Poisson equation is solved for the potential $\phi(x)$ using the Green's function solution,

$$\phi(x) = \frac{4\pi}{L}\left\{\left(\frac{L}{2} - x\right)\int_{-L/2}^{x}\left(\frac{L}{2} + x'\right)\rho(x')\,\mathrm{d}x' + \left(\frac{L}{2} + x\right)\int_{x}^{L/2}\left(\frac{L}{2} - x'\right)\rho(x')\,\mathrm{d}x'\right\}, \tag{A 2}$$

where the charge density is computed by

$$\rho(x) = \sum_s \int \mathrm{d}v\, q_s f_s(x, v). \tag{A 3}$$

Table 2 presents the dimensionless normalizations of the quantities in the code and the definitions of characteristic plasma parameters. Note the velocity coordinate normalization is species dependent, so the ion and electron distribution functions cover different absolute values of the velocity depending on the ion-to-electron mass ratio m_i/m_e and ion-to-electron temperature ratio T_i/T_e. For all of the examples presented in this paper, the equilibrium distribution function is specified as a Maxwellian,

$$f_{s0} = \frac{n_0}{(2\pi)^{1/2} v_{ts}} \mathrm{e}^{-v^2/2v_{ts}^2}, \tag{A 4}$$

although the code itself admits an arbitrary form of the equilibrium distribution function. A particularly useful relation in manipulating the normalizations is $v_{te} = \lambda_{de}\omega_{pe}$.

The plasma is assumed to be a fully ionized plasma with all ions in a singly charged state, so $n_{0e} = n_{0i} \equiv n_0$ and $q_e = -q_i$. Under these conditions, the linear Vlasov–Poisson dispersion relation yields the complex frequency ω_c as a function of three dimensionless parameters

$$\omega_c/\omega_{pe} = \overline{\omega}(k\lambda_{de}, T_i/T_e, m_i/m_e). \tag{A 5}$$

https://doi.org/10.1017/S0022377816001197 Published online by Cambridge University Press

Quantity	Normalization	Quantity	Definition
Position	$\hat{x} = x/\lambda_{de}$	Debye length	$\lambda_{de}^2 = T_e/4\pi n_0 q_e^2$
Velocity	$\hat{v}_s = v/v_{ts}$	Thermal velocity	$v_{ts}^2 = T_s/m_s$
Time	$\hat{t} = \omega_{pe} t$	Plasma frequency	$\omega_{pe}^2 = 4\pi n_0 q_e^2/m_e$
Potential	$\hat{\phi} = q_e \phi/T_e$		
Distribution	$\hat{f}_{s0} = f_{s0} v_{ts}/n_0$		

TABLE 2. Dimensionless normalization of quantities and definitions of plasma parameters in cgs units. The Boltzmann constant is absorbed into temperature, giving temperature in units of energy.

A recent paper (Pezzi, Camporeale & Valentini 2016) has explored the issue of numerical recurrence in the collisionless Vlasov–Poisson system, a numerical artefact arising from the discrete nature of the velocity-space resolution. The recurrence time is given by

$$T_{rec} = \frac{2\pi}{k\Delta v}, \tag{A 6}$$

which leads to a condition in our code normalization

$$\omega_{pe} T_{rec} = \frac{\pi n_v}{k\lambda_{de}(v_{max}/v_{te})}. \tag{A 7}$$

Care is taken to ensure that the number of velocity-space points n_v is chosen to be large enough that the recurrence time is longer than the simulation run time.

A.1. *Initialization of simulations*

In this paper, we initialize two different types of simulations: (i) a standing Langmuir wave pattern, and (ii) a propagating single Langmuir wave mode.

For the standing Langmuir wave pattern with a corresponding wavenumber given by $k\lambda_{de}$, a single wavelength of the wave pattern is created in VP by initializing a plasma with a constant ion density and a sinusoidal perturbation of the electron density $n_e(x) = n_0 + \delta n \sin(kx)$. The initial velocity distributions for both plasma species are Maxwellian distributions with relative temperatures given by the temperature ratio T_i/T_e. The initial perturbation of the electron distribution function is initialized in the variable δf_{eWl}, with $\delta f_{eB} = \delta f_{eWn} = 0$. The electric field arising from the sinusoidal electron density perturbation, computed from the Green's function solution using $f_e(x, v, t)$ and $f_i(x, v, t)$, leads to two equal-amplitude, counterpropagating Langmuir waves of wavenumber $k\lambda_{de}$ that constructively interfere to generate a standing wave pattern.

For the propagating single wave mode, the linear dispersion relation for Langmuir waves is solved in Fourier space for a specified wavenumber $k\lambda_{de}$,

$$D(\omega_c, k\lambda_{de}, T_i/T_e, m_i/m_e) = 1 - \frac{1}{k^2\lambda_{de}^2} \sum_s \frac{T_e}{T_s}[1 + \xi_s Z(\xi_s)] = 0. \tag{A 8}$$

This equation is solved numerically for complex frequency $\omega_c = \omega + \mathrm{i}\gamma$, where $\xi_s = \omega_c/(kv_{ts}\sqrt{2})$ and Z is the plasma dispersion function (Fried & Conte 1961). This complex ω_c is then used to initialize the Fourier coefficients of the linearized

https://doi.org/10.1017/S0022377816001197 Published online by Cambridge University Press

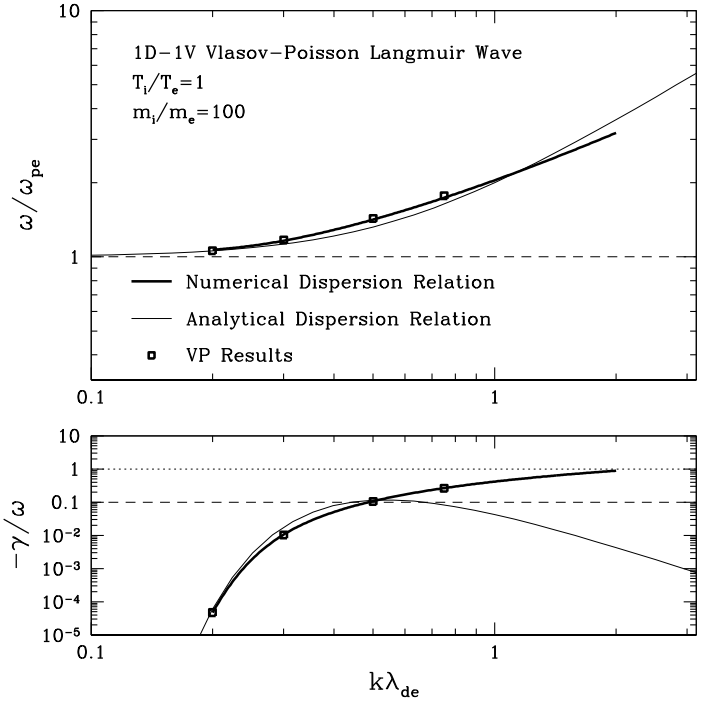

FIGURE 25. Validation of the Vlasov–Poisson simulation code VP for the normalized frequency and damping rate of Langmuir waves as a function of $k\lambda_{de}$. We show numerical solutions of the linear Vlasov–Poisson dispersion relation (thick lines), the analytical estimates from (A 10) and (A 11) (thin lines), and the numerical simulation results from VP using a standing Langmuir wave pattern generated by an initial electron density fluctuation (black boxes). Parameters for this case are $T_i/T_e = 1$ and $m_i/m_e = 100$.

perturbation of the distribution function for each species s for wave mode k,

$$\delta\hat{f}_{sWl}(k, v, 0) = \left(\frac{q_s\phi_1}{T_s}\right)\frac{kv}{\omega_c - kv}f_{s0}(v) \tag{A 9}$$

with initial wave amplitude of the potential given by the value of $q_e\phi_1/T_e$. The initialized perturbation is $f_{sWl}(x, v, 0) = \mathrm{Re}[\delta\hat{f}_{sWl}\mathrm{e}^{\mathrm{i}kx}]$, and $\delta f_{eB} = \delta f_{eWn} = 0$. The discrete nature of the velocity grid means that potentially sharp gradients may arise near the resonance at $v = \omega/k$, and this may lead to transient behaviour at the beginning of the simulation due to the fact that the discrete eigenfunction is not exactly that of a single propagating Langmuir wave. We have found that a practical procedure for reducing this transient behaviour is to smooth the initial δf_{sWl} for both species using a Crank–Nicholson diffusion operator in velocity space. This operator is applied N_s times successively with diffusion coefficient $\nu/(\Delta v)^2$ before the simulation is started. This procedure enables a single Langmuir wave propagating in one direction to be initialized.

A.2. *Code validation*

As a validation of VP, we have performed tests of the linear frequencies and damping rates of Langmuir waves with a range of values of $k\lambda_{de}$ for fully ionized, single species plasma with Maxwellian equilibrium velocity distribution functions and plasma parameters $T_i/T_e = 1$ and $m_i/m_e = 100$, as presented in figure 25. Both nonlinear

https://doi.org/10.1017/S0022377816001197 Published online by Cambridge University Press

simulations at sufficiently small initial amplitude $\delta n/n_0$ and linear simulations (where the nonlinear wave–particle interaction term is not included in the evolution) yield consistent results, given by the open squares, showing good agreement with the results of a numerical solution of the linear dispersion relation (thick lines). Also plotted (thin lines) for comparison are analytical estimates of the frequency ω and damping rate $-\gamma$ for Langmuir waves using the weak growth rate approximation,

$$\omega^2 = \omega_{pe}^2(1 + 3k^2\lambda_{de}^2), \tag{A 10}$$

$$\gamma = -\sqrt{\frac{\pi}{8}}\frac{\omega_{pe}}{|k\lambda_{de}|^3}\exp\left(\frac{-1}{2k^2\lambda_{de}^2} - \frac{3}{2}\right). \tag{A 11}$$

Appendix B. Simple model of normalized field–particle correlation

The linearized 1D-1V Vlasov–Poisson equations can be solved by a Laplace–Fourier transform approach to obtain the linear dispersion relation $D(\omega_c, k)$. This dispersion relation can be solved to obtain the complex frequency $\omega_c = \omega + \mathrm{i}\gamma$ for each possible linear wave mode with a given wavenumber k. From this linear solution for the complex frequency, we may determine the complex coefficients of the electrostatic potential of the wave $\tilde{\phi}(k, \omega_c)$ and of the perturbation to the distribution function for each species s, $\delta\tilde{f}_s(k, v, \omega_c)$, where the spatial and temporal variation is given by the usual form $\phi(x, t) = \mathrm{Re}[\tilde{\phi}(k, \omega_c)\mathrm{e}^{\mathrm{i}(kx-\omega_c t)}]$. The linear solution for the distribution function yields

$$\delta\tilde{f}_s(k, v, \omega_c) = \frac{q_s\tilde{\phi}(k, \omega_c)}{T_s}\frac{kv}{\omega_c - kv}f_{0s}(v) \tag{B 1}$$

in terms of a specified $\tilde{\phi}(k, \omega_c)$. The electric field is given by $\tilde{E}(k, \omega_c) = -\mathrm{i}k\tilde{\phi}(k, \omega_c)$.

Here we show how the normalized correlation between the fields and particles for a linear wave is simply a function of the normalized damping rate $-\gamma/\omega$ and the wave phase velocity $v_p = \omega/k$. Specifically, let us consider the normalized version of the correlation $C_{2norm}(q_s v\delta f_s(x_0, v, t), E(x_0, t))$. For two real variables of the form $A(t) = \mathrm{Re}[\tilde{A}(\omega_c)\mathrm{e}^{-\mathrm{i}\omega_c t}]$, the normalized correlation over one period, $\tau = 2\pi/\omega$, is given by $C(\tilde{A}, \tilde{B}) = (\tilde{A}\tilde{B}^* + \tilde{A}^*\tilde{B})/(2|\tilde{A}||\tilde{B}|)$, where $\tilde{A}$ and $\tilde{B}$ are complex coefficients.

The calculation is simplified by expressing the complex coefficients $\delta\tilde{f}_s(k, v, \omega_c)$ and $\tilde{E}(k, \omega_c)$ in polar form. We choose the phase of the linear wave solution by setting the complex coefficient of the potential to be a real constant, $\tilde{\phi}(k, \omega_c) = \phi_0$. In polar form, the electric field is represented by $\tilde{E} = -\mathrm{i}k\phi_0 = [k\phi_0]\mathrm{e}^{-\mathrm{i}\pi/2}$. The perturbed distribution function is given by

$$\delta\tilde{f}_s = \left(\frac{q_s\phi_0}{T_s}\right)\frac{kv}{(\omega - kv) + \mathrm{i}\gamma}f_{0s}(v), \tag{B 2}$$

where the phase of the perturbed distribution function, relative to ϕ_0, is determined by the magnitudes of the real frequency ω and damping rate γ. Expressing this complex coefficient in polar form yields

$$\delta\tilde{f}_s(k, v, \omega_c) = \left[\left(\frac{q_s\phi_0}{T_s}\right)\frac{kv}{\sqrt{(\omega - kv)^2 + \gamma^2}}f_{0s}(v)\right]\mathrm{e}^{\mathrm{i}\alpha}, \tag{B 3}$$

https://doi.org/10.1017/S0022377816001197 Published online by Cambridge University Press

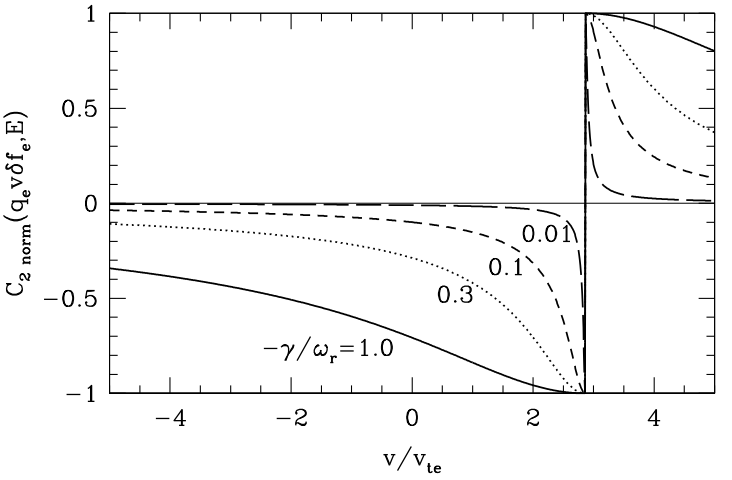

FIGURE 26. The normalized correlation $C_{2norm}(q_e v\delta f_e,\ E)$ for different values of $-\gamma/\omega = 0.01,\ 0.1,\ 0.3{,}1$, where the resonant phase velocity is given by $v_p = \omega/k = 2.86 v_{te}$.

where the phase is given by

$$\alpha = \tan^{-1}\left(\frac{-\gamma}{\omega - kv}\right). \tag{B 4}$$

Now, to evaluate the normalized correlation $C_{2norm}(q_s v\delta f_s(x_0, v, t), E(x_0, t))$, we have treat the sign of q_s carefully to get the change in the sign of the correlation between species. We choose to write $q_s = (-1)^{\delta_{se}}|q_s|$, where δ_{se} is the Kronecker delta, with the value 0 for $s = i$ and 1 for $s = e$. In this case, the contribution to the phase from the sign of q is given by $i\pi\delta_{se}$. Evaluating the normalized correlation, we obtain

$$C_{2norm}(q_s v\delta f_s(x_0, v, t), E(x_0, t)) = \cos(\alpha - \pi/2 + \pi\delta_{se}) = (-1)^{\delta_{se}} \sin(\alpha). \tag{B 5}$$

Manipulating the argument of the $\tan^{-1}$ yields a particularly illuminating form of the normalized correlation,

$$C_{2norm}(q_s v\delta f_s, E) = (-1)^{\delta_{se}} \sin\left[\tan^{-1}\left(\frac{-\gamma/\omega}{1 - v/v_p}\right)\right]. \tag{B 6}$$

One can see that the form of the normalized correlation is a simple function of the normalized damping rate $-\gamma/\omega$, where the sign of the correlation is expected to change at the resonant phase velocity $v = v_p = \omega/k$.

We plot the normalized correlation $C_{2norm}(-|q_e| v\delta f_e(x_0, v, t), E(x_0, t))$ for electrons in figure 26 for the case of a wave phase velocity $v_p = \omega/k = 2.86 v_{te}$ and for different values of the normalized damping rate $-\gamma/\omega = 0.01, 0.1, 0.3, 1$. Note that the case of the Langmuir wave with $k\lambda_{de} = 0.5$ has $-\gamma/\omega \simeq 0.11$. This simple calculation shows that the correlation of electrons with a linear Langmuir wave yields a change of sign through the resonant phase velocity, with the distribution function losing energy at lower velocities and gaining energy at higher velocities. Note that this strictly linear calculation does not correspond directly to figure 15 because the nonlinear evolution of the distribution function can alter the resulting normalized correlations

https://doi.org/10.1017/S0022377816001197 Published online by Cambridge University Press

substantially from this simple linear case. Nonetheless, this simple model provides a clear indication that the phase relationship between the electric field and the fluctuations in the distribution function, which depends on the velocity v, plays a key role in determining the energy transfer between fields and particles.

REFERENCES

ANDERSON, R. R. & MAEDA, K. 1977 VLF emissions associated with enhanced magnetospheric electrons. *J. Geophys. Res.* **82**, 135–146.

BALE, S. D., GOETZ, K., HARVEY, P. R., TURIN, P., BONNELL, J. W., DUDOK DE WIT, T., ERGUN, R. E., MACDOWALL, R. J., PULUPA, M., ANDRE, M. *et al.* 2016 The FIELDS Instrument Suite for Solar Probe Plus. *Space Sci. Rev* **204** (1), 49–82.

BARNES, A. 1966 Collisionless damping of hydromagnetic waves. *Phys. Fluids* **9**, 1483–1495.

BOROVSKY, J. E. & DENTON, M. H. 2011 No evidence for heating of the solar wind at strong current sheets. *Astrophys. J. Lett.* **739**, L61.

BOUROUAINE, S. & CHANDRAN, B. D. G. 2013 Observational test of stochastic heating in low-β fast-solar-wind streams. *Astrophys. J.* **774**, 96.

BOUROUAINE, S., MARSCH, E. & VOCKS, C. 2008 On the efficiency of nonresonant ion heating by coronal Alfvén waves. *Astrophys. J. Lett.* **684**, L119–L122.

BURCH, J. L., MOORE, T. E., TORBERT, R. B. & GILES, B. L. 2016 Magnetospheric multiscale overview and science objectives. *Space Sci. Rev.* **199**, 5–21.

BURKE, W. J., GOUGH, M. P., GENTILE, L. C., HUANG, C. Y., MACHUZAK, J. S. & RUBIN, A. G. 1999 MHz and kHz modulations of particle fluxes during beam experiments of the tethered satellite system missions. *Adv. Space Res.* **24**, 1047–1054.

BURTON, R. K. & HOLZER, R. E. 1974 The origin and propagation of chorus in the outer magnetosphere. *J. Geophys. Res.* **79**, 1014–1023.

CHANDRAN, B. D. G. 2010 Alfvén-wave turbulence and perpendicular ion temperatures in coronal holes. *Astrophys. J.* **720**, 548–554.

CHANDRAN, B. D. G., DENNIS, T. J., QUATAERT, E. & BALE, S. D. 2011 Incorporating kinetic physics into a two-fluid solar-wind model with temperature anisotropy and low-frequency Alfvén-wave turbulence. *Astrophys. J.* **743**, 197.

CHANDRAN, B. D. G., LI, B., ROGERS, B. N., QUATAERT, E. & GERMASCHEWSKI, K. 2010 Perpendicular ion heating by low-frequency Alfvén-wave turbulence in the solar wind. *Astrophys. J.* **720**, 503–515.

CHASTON, C. C. 2006 ULF waves and auroral electrons. In *Magnetospheric ULF Waves: Synthesis and New Directions* (ed. K. Takahashi, P. J. Chi, R. E. Denton & R. L. Lysak), Washington DC American Geophysical Union Geophysical Monograph Series, vol. 169, p. 239. American Geophysical Union.

CHASTON, C. C., BONNELL, J. W., CARLSON, C. W., MCFADDEN, J. P., ERGUN, R. E. & STRANGEWAY, R. J. 2003 Properties of small-scale Alfvén waves and accelerated electrons from FAST. *J. Geophys. Res.* **108**, 8003.

CHASTON, C. C., CARLSON, C. W., MCFADDEN, J. P., ERGUN, R. E. & STRANGEWAY, R. J. 2007 How important are dispersive Alfvén waves for auroral particle acceleration? *Geophys. Res. Lett.* **34**, 7101.

CHEN, C. H. K., BALE, S. D., SALEM, C. & MOZER, F. S. 2011 Frame dependence of the electric field spectrum of solar wind turbulence. *Astrophys. J. Lett.* **737**, L41.

CHEN, C. H. K., BOLDYREV, S., XIA, Q. & PEREZ, J. C. 2013 Nature of subproton scale turbulence in the solar wind. *Phys. Rev. Lett.* **110** (22), 225002.

CHEN, L., LIN, Z. & WHITE, R. 2001 On resonant heating below the cyclotron frequency. *Phys. Plasmas* **8**, 4713–4716.

COLEMAN, P. J. JR. 1968 Turbulence, viscosity, and dissipation in the solar-wind plasma. *Astrophys. J.* **153**, 371–388.

https://doi.org/10.1017/S0022377816001197 Published online by Cambridge University Press

DENSKAT, K. U., BEINROTH, H. J. & NEUBAUER, F. M. 1983 Interplanetary magnetic field power spectra with frequencies from 2.4 × 10 to the -5th HZ to 470 HZ from HELIOS-observations during solar minimum conditions. *J. Geophys. Zeit. Geophys.* **54**, 60–67.

DMITRUK, P., MATTHAEUS, W. H. & SEENU, N. 2004 Test particle energization by current sheets and nonuniform fields in magnetohydrodynamic turbulence. *Astrophys. J.* **617**, 667–679.

ERGUN, R. E., CARLSON, C. W., MCFADDEN, J. P., CLEMMONS, J. H. & BOEHM, M. H. 1991*a* Langmuir wave growth and electron bunching – results from a wave–particle correlator. *J. Geophys. Res.* **96**, 225–238.

ERGUN, R. E., CARLSON, C. W., MCFADDEN, J. P., TONTHAT, D. M. & CLEMMONS, J. H. 1991*b* Observation of electron bunching during Landau growth and damping. *J. Geophys. Res.* **96**, 11.

ERGUN, R. E., CARLSON, C. W., MOZER, F. S., DELORY, G. T., TEMERIN, M., MCFADDEN, J. P., PANKOW, D., ABIAD, R., HARVEY, P., WILKES, R. *et al.* 2001 The FAST satellite fields instrument. *Space Sci. Rev.* **98**, 67–91.

ERGUN, R. E., MCFADDEN, J. P. & CARLSON, C. W. 1998 *Wave–Particle Correlator Instrument Design*, Washington DC American Geophysical Union Geophysical Monograph Series, vol. 102, p. 325. American Geophysical Union.

FREDRICKS, R. W. & SCARF, F. L. 1973 Recent studies of magnetospheric electric field emissions above the electron gyrofrequency. *J. Geophys. Res.* **78**, 310–314.

FRIED, B. D. & CONTE, S. D. 1961 *The Plasma Dispersion Function*. Academic.

FUKUHARA, H., KOJIMA, H., UEDA, Y., OMURA, Y., KATOH, Y. & YAMAKAWA, H. 2009 A new instrument for the study of wave–particle interactions in space: one-chip wave–particle interaction analyzer. *Earth Planets Space* **61**, 765–778.

GARY, S. P. 1999 Collisionless dissipation wavenumber: linear theory. *J. Geophys. Res.* **104**, 6759–6762.

GOERTZ, C. K. & BOSWELL, R. W. 1979 Magnetosphere-ionosphere coupling. *J. Geophys. Res.* **84**, 7239–7246.

GOLDSTEIN, M. L., ROBERTS, D. A. & FITCH, C. A. 1994 Properties of the fluctuating magnetic helicity in the inertial and dissipation ranges of solar wind turbulence. *J. Geophys. Res.* **99**, 11519–11538.

GOUGH, M. P. 1980 A technique for rocket-borne detection of electron bunching at megahertz frequencies. *Nucl. Instrum. Meth.* **177**, 581–587.

GOUGH, M. P., BUCKLEY, A. M., CAROZZI, T. & BELOFF, N. 2003 Experimental studies of wave–particle interactions in space using particle correlators: results and future developments. *Adv. Space Res.* **32**, 407–416.

GOUGH, M. P., BURKE, W. J., HARDY, D. A., HUANG, C. Y., GENTILE, L. C., RUBIN, A. G., OBERHARDT, M. R., DROBOT, A. T., THOMPSON, D. C. & RAITT, W. J. 1998*a* Megahertz electron modulations during TSS 1R. *Geophys. Res. Lett.* **25**, 441–444.

GOUGH, M. P., CHRISTIANSEN, P. J. & WILHELM, K. 1990 Auroral beam-plasma interactions – particle correlator investigations. *J. Geophys. Res.* **95**, 12287–12294.

GOUGH, M. P., HARDY, D. A., BURKE, W. J., OBERHARDT, M. R., GENTILE, L. C., HUANG, C. Y., COOKE, D. L., RAITT, W. J., THOMPSON, D. C. & MCNEIL, W. 1997 Heating and low-frequency modulation of electrons observed during electron beam operations on TSS 1. *J. Geophys. Res.* **102**, 17335–17358.

GOUGH, M. P., HARDY, D. A. & JAMES, H. G. 1998*b* First results from the energetic particle instrument on the OEDIPUS-C sounding rocket. *Adv. Space Res.* **21**, 705–708.

GOUGH, M. P., HARDY, D. A., OBERHARDT, M. R., BURKE, W. J., GENTILE, L. C., MCNEIL, B., BOUNAR, K., THOMPSON, D. C. & RAITT, W. J. 1995 Correlator measurements of megahertz wave–particle interactions during electron beam operations on STS 46. *J. Geophys. Res.* **100**, 21561–21576.

GOUGH, M. P., HARDY, D. A., OBERHARDT, M. R., BURKE, W. J., GENTILE, L. C., THOMPSON, D. C. & RAITT, W. J. 1998*c* Spree measurements of wave–particle interactions generated by the electron guns on TSS-1 and TSS-1R. *Adv. Space Res.* **21**, 729–733.

GOUGH, M. P., MARTELLI, G., SMITH, P. N., MAEHLUM, B. N. & VENTURA, G. 1980 Bunching of 8–10 keV auroral electrons near an artificial electron beam. *Nature* **287**, 15–17.

GOUGH, M. P. & URBAN, A. 1983 Auroral beam/plasma interaction observed directly. *Planet. Space Sci.* **31**, 875–883.

HASEGAWA, A. 1976 Particle acceleration by MHD surface wave and formation of aurora. *J. Geophys. Res.* **81**, 5083–5090.

HOLLWEG, J. V. & ISENBERG, P. A. 2002 Generation of the fast solar wind: a review with emphasis on the resonant cyclotron interaction. *J. Geophys. Res. (Space Physics)* **107**, 1147.

HOWES, G. G. 2015 A dynamical model of plasma turbulence in the solar wind. *Phil. Trans. R. Soc. Lond.* A **373** (2041), 20140145.

HOWES, G. G. 2015 Kinetic turbulence. In *Magnetic Fields in Diffuse Media*, Springer.

HOWES, G. G. 2016 The Dynamical Generation of Current Sheets in Astrophysical Plasma Turbulence. *Astrophys. J. Lett.* **827**, L28.

HOWES, G. G., BALE, S. D., KLEIN, K. G., CHEN, C. H. K., SALEM, C. S. & TENBARGE, J. M. 2012 The slow-mode nature of compressible wave power in solar wind turbulence. *Astrophys. J. Lett.* **753**, L19.

HOWES, G. G., COWLEY, S. C., DORLAND, W., HAMMETT, G. W., QUATAERT, E. & SCHEKOCHIHIN, A. A. 2006 Astrophysical gyrokinetics: basic equations and linear theory. *Astrophys. J.* **651**, 590–614.

HOWES, G. G., COWLEY, S. C., DORLAND, W., HAMMETT, G. W., QUATAERT, E. & SCHEKOCHIHIN, A. A. 2008*a* A model of turbulence in magnetized plasmas: implications for the dissipation range in the solar wind. *J. Geophys. Res.* **113** (A12), A05103.

HOWES, G. G., DORLAND, W., COWLEY, S. C., HAMMETT, G. W., QUATAERT, E., SCHEKOCHIHIN, A. A. & TATSUNO, T. 2008*b* Kinetic simulations of magnetized turbulence in astrophysical plasmas. *Phys. Rev. Lett.* **100** (6), 065004.

HOWES, G. G., KLEIN, K. G. & TENBARGE, J. M. 2014 Validity of the Taylor hypothesis for linear kinetic waves in the weakly collisional solar wind. *Astrophys. J.* **789**, 106.

HOWES, G. G., TENBARGE, J. M., DORLAND, W., QUATAERT, E., SCHEKOCHIHIN, A. A., NUMATA, R. & TATSUNO, T. 2011 Gyrokinetic simulations of solar wind turbulence from ion to electron scales. *Phys. Rev. Lett.* **107**, 035004.

HUANG, C. Y., BURKE, W. J., HARDY, D. A., GOUGH, M. P., JAMES, H. G., VILLALÓN, E. & GENTILE, L. C. 2001 Electron acceleration by megahertz waves during OEDIPUS C. *J. Geophys. Res.* **106**, 1835–1848.

HUANG, C. Y., BURKE, W. J., HARDY, D. A., GOUGH, M. P., OLSON, D. G., GENTILE, L. C., GILCHRIST, B. E., BONIFAZI, C., RAITT, W. J. & THOMPSON, D. C. 1998 Cerenkov emissions of ion acoustic-like waves generated by electron beams emitted during TSS 1R. *Geophys. Res. Lett.* **25**, 721–724.

HUI, C.-H. & SEYLER, C. E. 1992 Electron acceleration by Alfven waves in the magnetosphere. *J. Geophys. Res.* **97**, 3953–3963.

ISENBERG, P. A. & HOLLWEG, J. V. 1983 On the preferential acceleration and heating of solar wind heavy ions. *J. Geophys. Res.* **88**, 3923–3935.

ISENBERG, P. A., LEE, M. A. & HOLLWEG, J. V. 2001 The kinetic shell model of coronal heating and acceleration by ion cyclotron waves: 1. Outward propagating waves. *J. Geophys. Res.* **106**, 5649–5660.

JOHNSON, J. R. & CHENG, C. Z. 2001 Stochastic ion heating at the magnetopause due to kinetic Alfvén waves. *Geophys. Res. Lett.* **28**, 4421–4424.

KARIMABADI, H., ROYTERSHTEYN, V., WAN, M., MATTHAEUS, W. H., DAUGHTON, W., WU, P., SHAY, M., LORING, B., BOROVSKY, J., LEONARDIS, E. *et al.* 2013 Coherent structures, intermittent turbulence, and dissipation in high-temperature plasmas. *Phys. Plasmas* **20** (1), 012303.

KASPER, J. C., ABIAD, R., AUSTIN, G., BALAT-PICHELIN, M., BALE, S. D., BELCHER, J. W., BERG, P., BERGNER, H., BERTHOMIER, M., BOOKBINDER, J. *et al.* 2015 Solar wind electrons alphas and protons (SWEAP) investigation: design of the solar wind and coronal plasma instrument suite for solar probe plus. *Space Sci. Rev.* **204**, 131–186. doi:10.1007/s11214-015-0206-3.

KATOH, Y., KITAHARA, M., KOJIMA, H., OMURA, Y., KASAHARA, S., HIRAHARA, M., MIYOSHI, Y., SEKI, K., ASAMURA, K., TAKASHIMA, T. *et al.* 2013 Significance of wave–particle interaction analyzer for direct measurements of nonlinear wave–particle interactions. *Ann. Geophys.* **31** (3), 503–512.

KEILING, A. 2009 Alfvén waves and their roles in the dynamics of the earth's magnetotail: a review. *Space Sci. Rev.* **142**, 73–156.

KEILING, A., WYGANT, J. R., CATTELL, C., PERIA, W., PARKS, G., TEMERIN, M., MOZER, F. S., RUSSELL, C. T. & KLETZING, C. A. 2002 Correlation of Alfvén wave Poynting flux in the plasma sheet at 4–7 R_E with ionospheric electron energy flux. *J. Geophys. Res.* **107**, 1132.

KENNEL, C. F. & PETSCHEK, H. E. 1966 Limit on stably trapped particle fluxes. *J. Geophys. Res.* **71**, 1.

KENNEL, C. F., SCARF, F. L., FREDRICKS, R. W., MCGEHEE, J. H. & CORONITI, F. V. 1970 VLF electric field observations in the magnetosphere. *J. Geophys. Res.* **75**, 6136–6152.

KIMURA, I., HASHIMOTO, K., MATSUMOTO, H., MUKAI, T., BELL, T. F., INAN, U. S., HELLIWELL, R. A. & KATSUFRAKIS, J. P. 1983 EXOS-B/Siple station VLF wave–particle interaction experiments. I – general description and wave–particle correlations. *J. Geophys. Res.* **88**, 282–294.

KLEIN, K. G., HOWES, G. G., TENBARGE, J. M., BALE, S. D., CHEN, C. H. K. & SALEM, C. S. 2012 Using synthetic spacecraft data to interpret compressible fluctuations in solar wind turbulence. *Astrophys. J.* **755**, 159.

KLEIN, K. G., HOWES, G. G., TENBARGE, J. M. & PODESTA, J. J. 2014 Physical interpretation of the angle-dependent magnetic helicity spectrum in the solar wind: the nature of turbulent fluctuations near the proton gyroradius scale. *Astrophys. J.* **785**, 138.

KLETZING, C. A. 1994 Electron acceleration by kinetic Alfvén waves. *J. Geophys. Res.* **99**, 11095–11104.

KLETZING, C. A., BOUNDS, S. R., LABELLE, J. & SAMARA, M. 2005 Observation of the reactive component of Langmuir wave phase-bunched electrons. *Geophys. Res. Lett.* **32**, L05106.

KLETZING, C. A. & MUSCHIETTI, L. 2006 Phase correlation of electrons and Langmuir waves. In *Geospace Electromagnetic Waves and Radiation* (ed. J. W. Labelle & R. A. Treumann), Lecture Notes in Physics, vol. 687, p. 313. Springer.

KRUSKAL, M. D. & OBERMAN, C. R. 1958 On the stability of plasma in static equilibrium. *Phys. Fluids* **1**, 275–280.

KULSRUD, R. M. 1983 Mhd description of plasma. In *Basic Plasma Physics I* (ed. A. A. Galeev & R. N. Sudan), Handbook of Plasma Physics, vol. 1, chap. 1.4, pp. 115–145. North Holland.

LANDAU, L. D. 1946 On the vibrations of the electronic plasma. *J. Phys.* **10**, 25.

LEAMON, R. J., MATTHAEUS, W. H., SMITH, C. W. & WONG, H. K. 1998*a* Contribution of cyclotron-resonant damping to kinetic dissipation of interplanetary turbulence. *Astrophys. J.* **507**, L181–L184.

LEAMON, R. J., MATTHAEUS, W. H., SMITH, C. W., ZANK, G. P., MULLAN, D. J. & OUGHTON, S. 2000 MHD-driven kinetic dissipation in the solar wind and corona. *Astrophys. J.* **537**, 1054–1062.

LEAMON, R. J., SMITH, C. W., NESS, N. F., MATTHAEUS, W. H. & WONG, H. K. 1998*b* Observational constraints on the dynamics of the interplanetary magnetic field dissipation range. *J. Geophys. Res.* **103**, 4775–4787.

LEAMON, R. J., SMITH, C. W., NESS, N. F. & WONG, H. K. 1999 Dissipation range dynamics: kinetic alfvén waves and the importance of β_e. *J. Geophys. Res.* **104**, 22331–22344.

LI, T. C., HOWES, G. G., KLEIN, K. G. & TENBARGE, J. M. 2016 Energy dissipation and Landau damping in two- and three-dimensional plasma turbulence. *Astrophys. J. Lett.* **832** (2), L24.

LYSAK, R. L. & DUM, C. T. 1983 Dynamics of magnetosphere-ionosphere coupling including turbulent transport. *J. Geophys. Res.* **88**, 365–380.

LYSAK, R. L. & LOTKO, W. 1996 On the kinetic dispersion relation for shear Alfvén waves. *J. Geophys. Res.* **101**, 5085–5094.

MANFREDI, G. 1997 Long-time behavior of nonlinear landau damping. *Phys. Rev. Lett.* **79**, 2815–2818.

MARKOVSKII, S. A. & VASQUEZ, B. J. 2011 A short-timescale channel of dissipation of the strong solar wind turbulence. *Astrophys. J.* **739**, 22.

MATTHAEUS, W. H. & VELLI, M. 2011 Who needs turbulence? A review of turbulence effects in the heliosphere and on the fundamental process of reconnection. *Space Sci. Rev.* **160**, 145–168.

MELROSE, D. B. 1986 *Instabilities in Space and Laboratory Plasmas*. Cambridge University Press.

MORRISON, P. J. 1994 The energy of perturbations for Vlasov plasmas. *Phys. Plasmas* **1**, 1447–1451.

MÜLLER, D., MARSDEN, R. G., ST. CYR, O. C. & GILBERT, H. R. 2013 Solar orbiter. Exploring the sun-heliosphere connection. *Sol. Phys.* **285**, 25–70.

MUSCHIETTI, L., ROTH, I. & ERGUN, R. 1994 Interaction of Langmuir wave packets with streaming electrons: phase-correlation aspects. *Phys. Plasmas* **1**, 1008–1024.

OLIVEN, M. N. & GURNETT, D. A. 1968 Microburst phenomena: 3. An association between microbursts and VLF chorus. *J. Geophys. Res.* **73**, 2355–2362.

O'NEIL, T. 1965 Collisionless damping of nonlinear plasma oscillations. *Phys. Fluids* **8**, 2255–2262.

OSMAN, K. T., KIYANI, K. H., CHAPMAN, S. C. & HNAT, B. 2014*a* Anisotropic intermittency of magnetohydrodynamic turbulence. *Astrophys. J. Lett.* **783**, L27.

OSMAN, K. T., MATTHAEUS, W. H., GOSLING, J. T., GRECO, A., SERVIDIO, S., HNAT, B., CHAPMAN, S. C. & PHAN, T. D. 2014*b* Magnetic reconnection and intermittent turbulence in the solar wind. *Phys. Rev. Lett.* **112** (21), 215002.

OSMAN, K. T., MATTHAEUS, W. H., GRECO, A. & SERVIDIO, S. 2011 Evidence for inhomogeneous heating in the solar wind. *Astrophys. J. Lett.* **727**, L11.

OSMAN, K. T., MATTHAEUS, W. H., HNAT, B. & CHAPMAN, S. C. 2012*a* Kinetic signatures and intermittent turbulence in the solar wind plasma. *Phys. Rev. Lett.* **108** (26), 261103.

OSMAN, K. T., MATTHAEUS, W. H., WAN, M. & RAPPAZZO, A. F. 2012*b* Intermittency and local heating in the solar wind. *Phys. Rev. Lett.* **108** (26), 261102.

PARK, C. G., PARKS, G. K. & LIN, C. S. 1981 A ground-satellite study of wave–particle correlations. *J. Geophys. Res.* **86**, 37–53.

PERRI, S., GOLDSTEIN, M. L., DORELLI, J. C. & SAHRAOUI, F. 2012 Detection of small-scale structures in the dissipation regime of solar-wind turbulence. *Phys. Rev. Lett.* **109** (19), 191101.

PEZZI, O., CAMPOREALE, E. & VALENTINI, F. 2016 Collisional effects on the numerical recurrence in Vlasov–Poisson simulations. *Phys. Plasmas* **23**, 022103.

QUATAERT, E. 1998 Particle heating by Alfvénic turbulence in hot accretion flows. *Astrophys. J.* **500**, 978–991.

QUATAERT, E. & GRUZINOV, A. 1999 Turbulence and particle heating in advection-dominated accretion flows. *Astrophys. J.* **520**, 248–255.

RETINÒ, A., SUNDKVIST, D., VAIVADS, A., MOZER, F., ANDRÉ, M. & OWEN, C. J. 2007 *In situ* evidence of magnetic reconnection in turbulent plasma. *Nat. Phys.* **3**, 236–238.

ROSENBERG, T. J., HELLIWELL, R. A. & KATSUFRAKIS, J. P. 1971 Electron precipitation associated with discrete very-low-frequency emissions. *J. Geophys. Res.* **76**, 8445–8452.

RUBIN, A. G., BURKE, W. J., GOUGH, M. P., MACHUZAK, J. S., GENTILE, L. C., HUANG, C. Y., HARDY, D. A., THOMPSON, D. C. & RAITT, W. J. 1999 Beam-induced electron modulations observed during TSS 1R. *J. Geophys. Res.* **104**, 17251–17262.

SALEM, C. S., HOWES, G. G., SUNDKVIST, D., BALE, S. D., CHASTON, C. C., CHEN, C. H. K. & MOZER, F. S. 2012 Identification of kinetic Alfvén wave turbulence in the solar wind. *Astrophys. J. Lett.* **745**, L9.

SCARF, F. L., FREDRICKS, R. W., KENNEL, C. F. & CORONITI, F. V. 1973 Satellite studies of magnetospheric substorms on August 15, 1968: 8. Ogo 5 plasma wave observations. *J. Geophys. Res.* **78**, 3119.

SCHEKOCHIHIN, A. A., COWLEY, S. C., DORLAND, W., HAMMETT, G. W., HOWES, G. G., QUATAERT, E. & TATSUNO, T. 2009 Astrophysical gyrokinetics: kinetic and fluid turbulent cascades in magnetized weakly collisional plasmas. *Astrophys. J. Suppl.* **182**, 310–377.

SCHRIVER, D., ASHOUR-ABDALLA, M., STRANGEWAY, R. J., RICHARD, R. L., KLEZTING, C., DOTAN, Y. & WYGANT, J. 2003 FAST/polar conjunction study of field-aligned auroral acceleration and corresponding magnetotail drivers. *J. Geophys. Res.* **108**, 8020.

SCHROEDER, J. W. R., SKIFF, F., KLETZING, C. A., HOWES, G. G., CARTER, T. A. & DORFMAN, S. 2016 Direct measurement of electron sloshing of an inertial Alfvén wave. *Geophys. Res. Lett.* **43**, 4701–4707.

SERVIDIO, S., GRECO, A., MATTHAEUS, W. H., OSMAN, K. T. & DMITRUK, P. 2011 Statistical association of discontinuities and reconnection in magnetohydrodynamic turbulence. *J. Geophys. Res.* **116**, 9102.

SHAW, R. R. & GURNETT, D. A. 1975 Electrostatic noise bands associated with the electron gyrofrequency and plasma frequency in the outer magnetosphere. *J. Geophys. Res.* **80**, 4259–4271.

SPIGER, R. J., MURPHREE, J. S., ANDERSON, H. R. & LOEWENSTEIN, R. F. 1976 Modulation of auroral electron fluxes in the frequency range 50 kHz to 10 MHz. *J. Geophys. Res.* **81**, 1269–1278.

SPIGER, R. J., OEHME, D., LOEWENSTEIN, R. F., MURPHREE, J., ANDERSON, H. R. & ANDERSON, R. 1974 A detector for high frequency modulation in auroral particle fluxes. *Rev. Sci. Instrum.* **45**, 1214–1220.

STASIEWICZ, K., BELLAN, P., CHASTON, C., KLETZING, C., LYSAK, R., MAGGS, J., POKHOTELOV, O., SEYLER, C., SHUKLA, P., STENFLO, L. *et al.* 2000 Small scale Alfvénic structure in the aurora. *Space Sci. Rev.* **92**, 423–533.

STIX, T. H. 1992 *Waves in Plasmas*. American Institute of Physics.

SUNDKVIST, D., RETINÒ, A., VAIVADS, A. & BALE, S. D. 2007 Dissipation in turbulent plasma due to reconnection in thin current sheets. *Phys. Rev. Lett.* **99** (2), 025004.

TAYLOR, G. I. 1938 The spectrum of turbulence. *Proc. R. Soc. Lond.* A **164**, 476–490.

TENBARGE, J. M. & HOWES, G. G. 2013 Current sheets and collisionless damping in kinetic plasma turbulence. *Astrophys. J. Lett.* **771**, L27.

TENBARGE, J. M., PODESTA, J. J., KLEIN, K. G. & HOWES, G. G. 2012 Interpreting magnetic variance anisotropy measurements in the solar wind. *Astrophys. J.* **753**, 107.

TOLD, D., JENKO, F., TENBARGE, J. M., HOWES, G. G. & HAMMETT, G. W. 2015 Multiscale nature of the dissipation range in gyrokinetic simulations of Alfvénic turbulence. *Phys. Rev. Lett.* **115** (2), 025003.

URITSKY, V. M., POUQUET, A., ROSENBERG, D., MININNI, P. D. & DONOVAN, E. F. 2010 Structures in magnetohydrodynamic turbulence: detection and scaling. *Phys. Rev.* E **82** (5), 056326.

VAIVADS, A., RETIN, A., SOUCEK, J., KHOTYAINTSEV, YU. V., VALENTINI, F., ESCOUBET, C. P., ALEXANDROVA, O., ANDR, M., BALE, S. D., BALIKHIN, M. *et al.* 2016 Turbulence heating observer satellite mission proposal. *J. Plasma Phys.* **82** (5), 905820501.

VILLANI, C. 2014 Particle systems and nonlinear Landau dampinga. *Phys. Plasmas* **21** (3), 030901.

VOITENKO, Y. & GOOSSENS, M. 2004 Excitation of kinetic Alfvén turbulence by MHD waves and energization of space plasmas. *Nonlinear Process. Geophys.* **11**, 535–543.

WAN, M., MATTHAEUS, W. H., KARIMABADI, H., ROYTERSHTEYN, V., SHAY, M., WU, P., DAUGHTON, W., LORING, B. & CHAPMAN, S. C. 2012 Intermittent dissipation at kinetic scales in collisionless plasma turbulence. *Phys. Rev. Lett.* **109** (19), 195001.

WANG, X., TU, C., HE, J., MARSCH, E. & WANG, L. 2013 On intermittent turbulence heating of the solar wind: differences between tangential and rotational discontinuities. *Astrophys. J. Lett.* **772**, L14.

WATKINS, N. W., BATHER, J. A., CHAPMAN, S. C., MOUIKIS, C. G., GOUGH, M. P., WYGANT, J. R., HARDY, D. A., COLLIN, H. L., JOHNSTONE, A. D. & ANDERSON, R. R. 1996 Suspected wave–particle interactions coincident with a pancake distribution as seen by the CRRES spacecraft. *Adv. Space Res.* **17**, 83–87.

WHITE, R., CHEN, L. & LIN, Z. 2002 Resonant plasma heating below the cyclotron frequency. *Phys. Plasmas* **9**, 1890–1897.

WOOLLISCROFT, L. J. C., ALLEYNE, H. S. C., DUNFORD, C. M., SUMNER, A., THOMPSON, J. A., WALKER, S. N., YEARBY, K. H., BUCKLEY, A., CHAPMAN, S. & GOUGH, M. P. 1997 The digital wave-processing experiment on cluster. *Space Sci. Rev.* **79**, 209–231.

WU, P., PERRI, S., OSMAN, K., WAN, M., MATTHAEUS, W. H., SHAY, M. A., GOLDSTEIN, M. L., KARIMABADI, H. & CHAPMAN, S. 2013 Intermittent heating in solar wind and kinetic simulations. *Astrophys. J. Lett.* **763**, L30.

ZHDANKIN, V., UZDENSKY, D. A. & BOLDYREV, S. 2015*a* Temporal analysis of dissipative structures in magnetohydrodynamic turbulence. *Astrophys. J.* **811**, 6.

ZHDANKIN, V., UZDENSKY, D. A. & BOLDYREV, S. 2015*b* Temporal intermittency of energy dissipation in magnetohydrodynamic turbulence. *Phys. Rev. Lett.* **114** (6), 065002.

ZHDANKIN, V., UZDENSKY, D. A., PEREZ, J. C. & BOLDYREV, S. 2013 Statistical analysis of current sheets in three-dimensional magnetohydrodynamic turbulence. *Astrophys. J.* **771**, 124.